Chapter 17

DOA Estimation of Nonstationary Signals

Moeness G. Amin and Yimin D. Zhang
Center for Advanced Communications
Villanova University, Villanova, PA 19085, USA

Abstract

In this Chapter, we discuss the direction finding problem of sources emitting or inducing nonstationary signals. The focus is on signals which are uniquely characterized by their instantaneous frequencies. Recognizing the quadratic time-frequency distributions as an effective tool to localize signal power in the time-frequency domain, we present nonstationary array processing in the context of time-frequency signal representations. The spatial time-frequency distribution (STFD) framework is used to re-introduce high-resolution direction-of-arrival estimation methods, in which a matrix of auto- and cross- bilinear distributions of the data observations across the array is used in lieu of the traditional covariance matrix. The high signal-to-noise ratio, achieved by selecting the entire, or part of the source time-frequency signatures, improves subspace and source angle estimations over covariance-based subspace methods. The Chapter discusses time-frequency MUSIC, time-frequency maximum likelihood, and time-frequency ESPRIT methods. It also uses the STFD framework for direction finding in multiple-input multiple-output (MIMO) configurations.

Glossary

- **Time-frequency distribution:** Distribution of the signal power over both the time and frequency variables.

- **Spatial time-frequency distribution:** A matrix whose entries are the time-frequency distributions associated with the outerproducts of the data observation vectors measured across a sensor array.

- **Auto-term:** A sample in the time-frequency domain which pertains to the time-frequency distribution of an individual component of the signal.
- **Cross-term:** An artifact in the time-frequency domain which is introduced by the bilinear product of two components of the input signal.
- **Source discrimination:** Isolation of individual source signals in single variable or joint-variables domains, such as time, frequency, space, and time-frequency domains.

17.1 Introduction

For many decades, time-frequency (t-f) signal representations, such as the Wigner-Ville distribution (WVD) and spectrograms, were only applied to analyze nonstationary signals incident on single-sensor receivers. The objective is to characterize the data observations in the t-f domain, leading to proper signal detection and characterization, separation, classification, and cancellation. These offerings were subsequently enhanced by introducing reduced interference quadratic time-frequency distributions (TFDs) which have led to improved multi-component signal power localizations in the t-f domain. With sensor arrays being ubiquitous in many application areas of signal processing, such as communications, radar, acoustic, and biomedical, it has become important to consider TFDs in the context of array processing. This is successfully achieved within the framework of spatial time-frequency distribution (STFD) [9–13, 75].

This Chapter discusses the direction-of-arrival (DOA) estimation of far-field sources producing nonstationary signals, particularly those in the form of frequency modulated (FM) waveforms. We use DOA estimation methods based on the quadratic (bilinear) STFD framework. Nonstationary signals are encountered in various passive and active arrays using different sensing modalities. For example, many modern radar systems use linear FM (LFM) signals to achieve pulse compression (LFM signals are also referred to as chirp signals). Alternatively, accelerating, rotating, or maneuvering targets generate time-varying Doppler frequencies, with well defined Doppler-frequency signatures [19, 53]. Further, FM signals can be easily generated and, as such, they are considered the preferred waveforms for smart jammers, and have proven effective in hindering and compromising communications and radar receivers [4].

The STFD framework was first developed by Belouchrani and Amin for the blind separation of narrowband nonstationary signals [12]. It was shown that the STFD matrix is related to the source TFD matrix by the spatial mixing matrix in a manner similar to the commonly used expression, in narrowband array processing problems, relating the sensor spatial covariance matrix to the source covariance matrix. The same STFD framework was then used for direction finding of nonstationary signals using t-f based DOA estimation approaches, such as t-f MUSIC, t-f root-MUSIC, t-f maximum likelihood (t-f ML), and t-f ESPRIT [8, 13, 31, 33, 59, 66, 74]. These techniques, when applied to the source t-f signatures, have shown improved performance, compared to conventional DOA estimation approaches. The latter, which directly operate on the data or its covariance matrix, do not account for, or properly utilize, the instantaneous frequency (IF) characterizations of the source signals. Comprehensive analyses, supporting STFD-based DOA estimations and demonstrating the robustness of the signal and noise subspaces associated with the STFD matrices, were provided by Zhang et al. [75]. It was shown that, signal-to-noise ratio (SNR) enhancement can be obtained from constructing the STFD matrix incorporating signal power concentration regions in the time-frequency domain. This, in turn, leads to robustness of the signal and noise subspace estimates compared to their counterparts, which are obtained using the data covariance matrix. In addition, masking and filtering of the source t-f signatures allow separation and, subsequently, the consideration of individual, or a subgroup of, sources in the field of view. With such source discriminatory capability, the receiver can handle and process

more signals than sensors. Reduction of sources further increases SNR and lowers the mutual interference between the signals, improveing signal and noise subspace estimations. In some applications, particularly when acoustic signals are involved, the TFD of multiple signals can be approximately disjoint or orthogonal, i.e., only one signal is present at a given t-f point. With a single source considered at a time, the source DOA can be estimated using only two receivers [55]. In essence, DOA estimation for nonstationary signals, which are well separated in the t-f domain, should be performed using t-f methods.

It is recognized that the advantages of t-f based DOA estimation can only be materialized if appropriate t-f points are selected in the formulation of the STFD matrices. While in some scenarios, the selection of t-f points of peak power may be relatively simple, the problem may become challenging in other situations, e.g., when the signals are highly contaminated by noise. Different approaches for t-f point selection are summarized in [14] and references therein. Utilization of the spatial degrees-of-freedom, or spatial diversity, embedded in the STFD matrix, can reduce noise and enhance the t-f signatures of the signals of interest without the need of using robust t-f kernels [3]. A simple example for achieving this task is through an average of the TFDs over all receive sensors [45]. Insights into the characteristics of TFDs corresponding to different sensors can also assist in the identification of auto-term and cross-term points [40, 68]. It is worthnoting that the separation of the auto-term t-f points from cross-term t-f points in general is less of an issue in DOA estimation than in blind source separation applications. This is because, in performing DOA estimation, STFD matrices only need to meet the full rank requirement [8]. This requirement can be satisfied with the inclusion of cross-terms. Nevertheless, the capability of separating auto-term points from cross-term points allows the selection of t-f regions corresponding to a subset of sources for proper source discrimination.

This Chapter focuses on the DOA estimation approaches of nonstationary signals based on the STFD framework. An analogous framework can be provided using linear transforms, such as the short-time Fourier transform (STFT) and wavelet transform, both can achieve power localization and SNR enhancement. However, multi-resolution analysis is not most effective when dealing with signals characterized by their IF laws, which is the assumption made throughout this Chapter. The STFT, on the other hand, has a well known shortcoming, trading off temporal and spectral resolutions, and its magnitude square is already considered within the STFD framework. Nevertheless, recent advances on the exploitation of fractional Fourier transform (FrFT) and signal stationarization for DOA estimations are considered in this chapter.

In addition to STFDs, we also review relevant recent approaches for nonstationary signal DOA estimations. One of these approaches is the exploitation of spatial joint-variable distributions (SJVD), such as spatial ambiguity function (SAF). The latter employs the Doppler and time-lag variables, in lieu of the time and frequency variables [6]. Another important extension of the STFD and SJVD based DOA estimation methods is the consideration of wideband signals where the narrowband assumption does not hold, i.e., the steering vector varies with the frequency within the signal bandwidth [31, 46, 48]. The latest application of STFD to multiple-input multiple-output (MIMO) radar systems for joint direction-of-departure (DOD) and DOA estimations [69] is also introduced.

The following notations are used in this Chapter. A lower (upper) case bold letter denotes a vector (matrix). E[$\cdot$] represents statistical mean operation. $(\cdot)^*$, $(\cdot)^T$ and $(\cdot)^H$ respectively denote complex conjugation, transpose, and conjugate transpose (Hermitian) operations. Re($\cdot$) represents the real part operation of a complex variable, vector or matrix. $\odot$ denotes the Hadamard product, $\otimes$ is the Kronecker product, and $\diamond$ denotes the Khatri-Rao product. $\mathbf{I}_n$ expresses the $n \times n$ identity matrix. Diag($\mathbf{x}$) denotes a diagonal matrix using the elements of $\mathbf{x}$ as its diagonal elements, diag($\mathbf{X}$) a vector consisting of the diagonal elements of matrix $\mathbf{X}$, and vec($\mathbf{X}$) a vectorized result of matrix $\mathbf{X}$. det($\cdot$) and tr($\cdot$) respectively denote the determinant and trace of a matrix. In addition, $\mathbb{C}^{N\times M}$ denotes the complete set of $N \times M$ complex entries, $[\mathbf{a}]_n$ denotes the nth element of vector $\mathbf{a}$, and $[\mathbf{A}]_{m,n}$ denotes the (m,n)th element of matrix $\mathbf{A}$. $\delta_{i,l}$ is the Kronecker delta function which

equals to 1 when $i = l$ and 0 otherwise.

17.2 Nonstationary Signals and Time-Frequency Representations

17.2.1 Nonstationary Signals

A large class of signal processing techniques deal with deterministic or stochastic time-domain signals that are stationary. A deterministic signal is said to be stationary if it can be written as a discrete sum of sinusoids, whereas in the random case, a signal $x(t)$ is said to be wide-sense stationary (or stationary up to the second order) if its expectation is independent of time, and its autocorrelation function $\mathrm{E}[x(t_1)x^*(t_2)]$ depends only on the time difference $t_2 - t_1$ [7]. For stationary signals, parameters such as the mean and variance, if they exist, also do not change over time or space. For this type of signals, the Fourier transform is widely used to extract the frequency-domain information from the time-domain signals and also as a pre-processing step for various temporal, spatial, and spatio-temporal processing methods.

Many real-world signals, however, are nonstationary. A signal is referred to as nonstationary if one of the fundamental assumptions of stationary signals is no longer valid. For example, a finite duration signal, in particular a transient signal (for which the length is short compared to the observation duration), is nonstationary. Also, many nonstationary signals have their frequency contents and properties change with time. Signals with time-varying spectra include: the impulse response of a wireless communication channel, radar and sonar acoustic waves, seismic acoustic waves, biomedical signals, such as electrocardiogram (ECG) or neonatal seizures, biological signals, such as bat or dolphin echolocation sounds, vocals in speech, notes in music, engine noise, shock waves in fault structures and jamming signals [49].

17.2.2 Cohen's Class of Time-Frequency Representations

There are a number of ways one can perform t-f analysis for nonstationary signals, most of which fall into the following two classes: linear t-f analysis and bilinear t-f analysis. Short-time Fourier transform (STFT), fractional Fourier transform (FrFT) and wavelet transform are commonly used techniques to perform linear t-f analysis [1, 7]. In contrast with linear t-f representations, which decompose the signal to basis functions, or elementary components (the atoms), the bilinear t-f representations, introduced in the following subsection, distribute the signal power over two description variables: time and frequency.

The Cohen's class of TFDs is the foundation of the STFD framework for direction finding as shown in Sections 17.3 and 17.4. The Cohen's class of auto-term TFDs of a narrowband signal $x(t)$ is defined as [22, 23],

$$D_{xx}(t,f) = \int_{-\infty}^{\infty}\int_{-\infty}^{\infty} \phi(t-u,\tau)x\left(u+\frac{\tau}{2}\right)x^*\left(u-\frac{\tau}{2}\right)e^{-j2\pi f\tau}dud\tau, \tag{17.1}$$

where t and f represent the time and frequency indexes, respectively, $\phi(t,\tau)$ is the t-f kernel, and τ is the time-lag variable.

The cross-term TFD of two signals $x_i(t)$ and $x_k(t)$ is defined as

$$D_{x_ix_k}(t,f) = \int_{-\infty}^{\infty}\int_{-\infty}^{\infty} \phi(t-u,\tau)x_i\left(u+\frac{\tau}{2}\right)x_k^*\left(u-\frac{\tau}{2}\right)e^{-j2\pi f\tau}dud\tau. \tag{17.2}$$

In practice, TFDs are often evaluated using their discrete-time forms [20]. To use integer time delay τ, we rewrite (17.1) as

$$D_{xx}(t,f) = 2\int_{-\infty}^{\infty}\int_{-\infty}^{\infty}\phi(t-u,2\tau)x(u+\tau)\,x^*(u-\tau)\,e^{-j4\pi f\tau}dud\tau. \tag{17.3}$$

The discrete form of the auto-term TFD corresponding to (17.3) is typically expressed as

$$D_{xx}(t,f) = \sum_{u=-\infty}^{\infty}\sum_{\tau=-\infty}^{\infty}\phi(t-u,\tau)x(u+\tau)\,x^*(u-\tau)\,e^{-j4\pi f\tau}, \tag{17.4}$$

which excludes the constant of two and a scaling factor in τ for expressional convenience. Similarly, the discrete-form of the cross-term TFD corresponding to (17.2) is given by

$$D_{x_ix_k}(t,f) = \sum_{u=-\infty}^{\infty}\sum_{\tau=-\infty}^{\infty}\phi(t-u,\tau)x_i(u+\tau)\,x_k^*(u-\tau)\,e^{-j4\pi f\tau}. \tag{17.5}$$

It is clear from the above equations that the TFD maps one-dimensional (1-D) signals in the time domain into two-dimensional (2-D) signal representations in the t-f domain. The fundamental TFD property of concentrating the input signal energy around its IF, while spreading the noise energy over the entire t-f domain, is crucial in DOA estimation, as it increases the effective SNR. For a single-component LFM signal, pseudo Wigner-Ville distribution (PWVD) can achieve SNR improvement up to the window length [75]. The SNR enhancement is dominantly determined by the window size, but is less sensitive to the type of t-f kernels [44]. When all the t-f points are selected within a 3-dB bandwidth from the peaks, the SNR improvement remains proportional to the window length [67]. Such observations are valid for a general class of signals, provided that the third-order derivative of the waveform phase is negligible or, equivalently, the waveforms can be approximated by an LFM within each sliding window interval.

The properties of a TFD can be characterized by simple constraints on the kernel. Different kernels can be designed and used to generate TFDs with prescribed, desirable properties. WVD is often regarded as the basic or prototype quadratic TFDs, since the other quadratic TFDs can be described as filtered version of the WVD. WVD is known to provide the best t-f resolution for single-component LFM signals, but it yields high cross-terms when the frequency law is nonlinear or when a multi-component signal is considered. Various reduced interference kernels have been developed to reduce the cross-term interference. Table 1 shows some commonly used kernel functions [19], where $\delta(t)$ is a Dirac delta function, rect(t) is a rectangular window function, $w(t)$ is an arbitrary window function, and σ and a are scalars. TFD examples that use these kernels are illustrated in the following two examples. In addition to these kernels that assume fixed parameters, some kernels, such as the adaptive optimal kernel, provide signal-adaptive filtering capability [17].

Examples

Figures 17.1(a) and 17.1(b) show the real- and imaginary-parts of an analytic LFM signal, expressed as $x(t) = \exp[j2\pi(0.1t + 0.001176t^2)$, $t = 0, ..., 255$. The start and end frequencies of the LFM signals are, respectively, 0.1 and 0.4. Performing Fourier transform of the signal yields a spectrum spreading over the normalized frequency band [0.1, 0.4], as shown in Figure 17.1(c). The WVD of the waveform, shown in Figure 17.1(d), depicts high energy concentration of the instantaneous narrowband signal with a linearly time-varying IF signature.

Figure 17.2 shows the t-f representations of two time-limited parallel LFM signals using different kernels. The WVD provides sharp auto-term signatures, whereas the cross-terms are evidently present in the middle of the two auto-term signatures. By using PWVD, the cross-terms in the time-domain are mitigated, whereas

Table 17.1: Example of time-frequency kernels

Distribution	**Kernel** $\phi(t,\tau)$
Wiger-Ville	$\delta(t)$
Pseudo Wigner-Ville	$\delta(t)w(\tau)$
Choi-Williams [25]	$\frac{\sqrt{\pi\sigma}}{\lvert\tau\rvert}\exp\left(-\frac{\pi^2\sigma t^2}{\tau^2}\right)$
Zhao-Atlas-Marks [72]	$w(\tau)\text{rect}\left(\frac{t}{2\tau/a}\right)$

the frequency-domain cross-terms remain. Both the Choi-Williams distribution and Zhao-Atlas-Marks distribution provide much reduced cross-term presence. The three non-WVD distributions yield much wider auto-term signatures in the t-f domain.

17.2.3 Wigner-Radon Transform and Fractional Fourier Transform for LFM Signals

The IFs of LFM (chirp) signals vary linearly with time. The WVD auto-terms of a chirp signal represent themselves in the t-f plane as a straight line with positive values. The time-varying frequency behavior of each LFM component can be described in the t-f domain by the slope (chirp rate) and the initial frequency. This property enables signal parameter estimation and characterizations. The Wigner-Radon transform and fractional Fourier transform (FrFT) are well known techniques that utilize these LFM signal properties. These techniques can be used for DOA estimation of LFM signals. FrFT-based DOA estimation is discussed in Section 17.4.4.

For an LFM signal $x(t)$, whose IF is expressed as $f(t) = f_0 + \beta t$, integrating the WVD $D_{xx}(t,f)$ over the t-f line segments yields high peak values, and thus allows estimation of the chirp rate β and the initial frequency f_0, which uniquely describe the signature of the LFM signal. The following line integration,

$$L(f_0,\beta) = \int D_{xx}(t, f_0 + \beta t)dt, \tag{17.6}$$

is referred to as the Wigner-Radon transform. The above integration is equivalent to dechirping, i.e., signal multiplication with the conjugation of the LFM signal, followed by power spectral calculation of the product [41, 62]. For multi-component LFM signals, the Wigner-Radon transform yields peaks in the respective (f_0,β) positions in the time-frequency plane, whereas the cross-terms are effectively mitigated due to their positive-negative oscillating behavior.

The FrFT, on the other hand, is a generalization of the classical Fourier transform. The FrFT was first developed for quantum mechanics [47], but has found broad applications since it was introduced to the signal processing community [1]. Reference [1] also analyzed the relationship between the FrFT and the WVD. FrFT is, in essence, a rotation of the signal representation in the t-f domain (Figure 17.3). The FrFT defines an operator, denoted as R^{α}, that performs counterclockwise rotation of the signal by an angle of α in the t-f plane. In this sense, the classical Fourier transform becomes a specific case by setting $\alpha = \pi/2$.

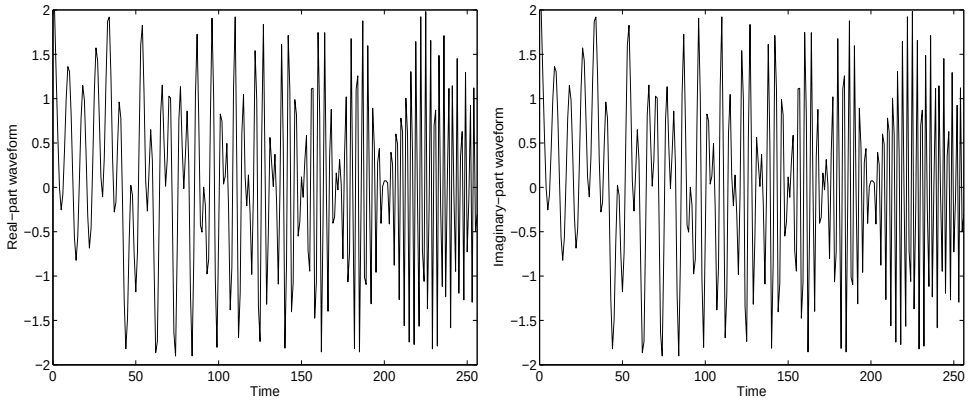

(a) Real-part of the waveform

(b) Imaginary-part of waveform

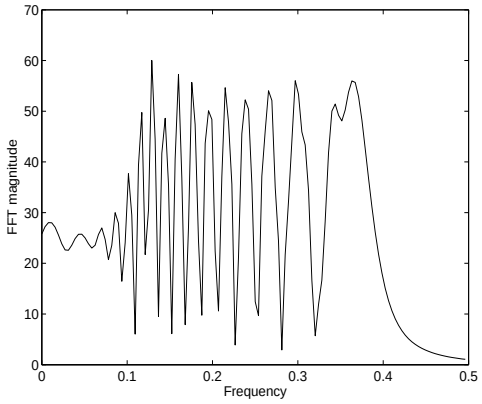

(c) FFT magnitude

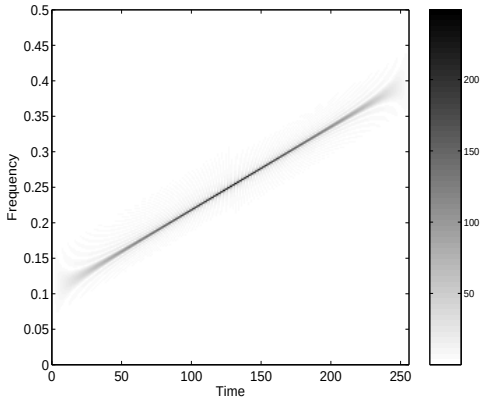

(d) Wigner-Ville distribution.

Figure 17.1: Waveform and Wigner-Ville distribution of an LFM signal.

The FrFT is defined by the following transformation kernel:

$$K_\alpha(t,u) = \begin{cases} \sqrt{\dfrac{1-j\cot\alpha}{2\pi}}\, e^{j\frac{t^2+u^2}{2}\cot\alpha - jut\csc\alpha}, & \text{if } \alpha \text{ is not a multiple of } \pi \\ \delta(t-u), & \text{if } \alpha \text{ is a multiple of } 2\pi \\ \delta(t+u), & \text{if } \alpha+\pi \text{ is a multiple of } 2\pi. \end{cases} \tag{17.7}$$

where u is the axis of the transformed domain. The FrFT of a signal $x(t)$ is then expressed as

$$\begin{aligned} X_\alpha(u) &= \mathrm{R}^\alpha x(t) = \int_{-\infty}^{\infty} x(t)K_\alpha(t,u)dt \\ &= \begin{cases} \sqrt{\dfrac{1-j\cot\alpha}{2\pi}}\, e^{j\frac{u^2}{2}\cot\alpha} \displaystyle\int_{-\infty}^{\infty} x(t)e^{j\frac{t^2}{2}\cot\alpha - jut\csc\alpha}dt, & \text{if } \alpha \text{ is not a multiple of } \pi \\ x(t), & \text{if } \alpha \text{ is a multiple of } 2\pi \\ x(-t), & \text{if } \alpha+\pi \text{ is a multiple of } 2\pi. \end{cases} \end{aligned} \tag{17.8}$$

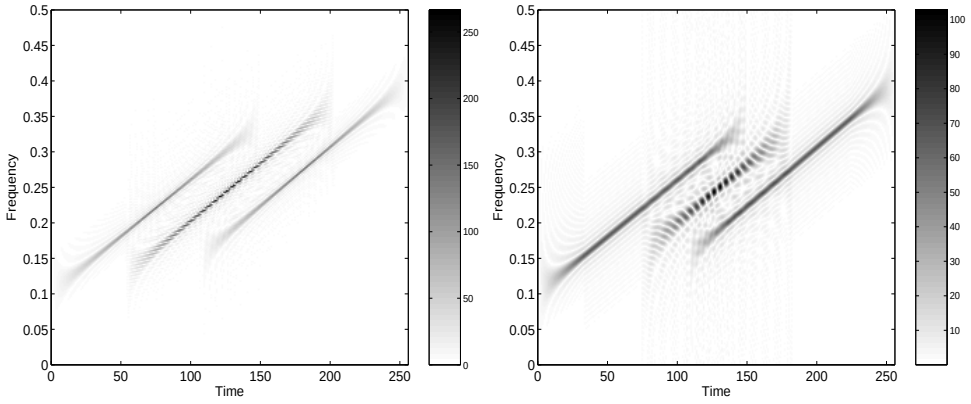

(a) Wigner-Ville distribution

(b) Pseudo Wigner-Ville distribution

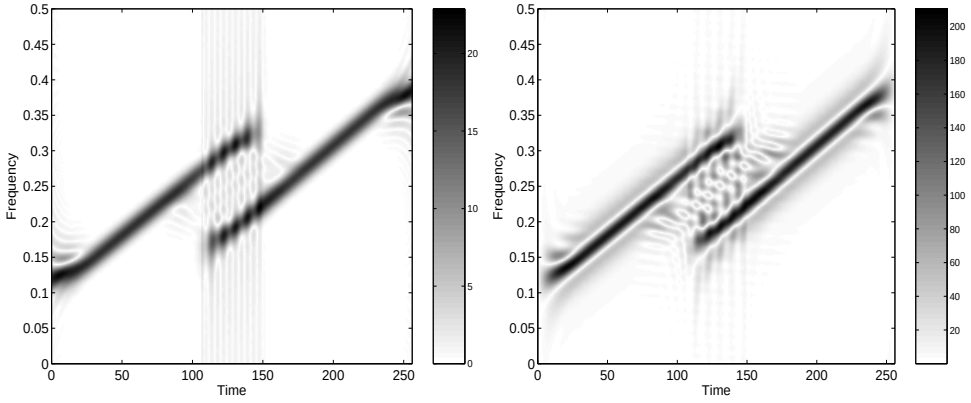

(c) Choi-Williams distribution

(d) Zhao-Atlas-Marks distribution.

Figure 17.2: TFDs of two LFM signals corresponding to different kernels.

By properly choosing the rotating angle, an LFM signal would be well localized in the transformed domain. Readers interested in this subject can refer to [28] for additional information about FrFT.

17.2.4 Polynomial Phase Signals and Parameter Estimations

A polynomial phase signal (PPS) is an extension of LFM signals which include higher phase orders. The parameter estimation of PPS signals can be used for DOA estimation through signal stationarization, as described in Section 17.4.4.

Mathematically, a PPS can be expressed as

$$x(t) = Ae^{j\phi(t)} = Ae^{j\sum_{k=0}^{K} a_k t^k}, \tag{17.9}$$

where K is the polynomial order of the phase $\phi(t)$, $\{a_0, ..., a_K\}$ are the polynomial coefficients, and A is the signal amplitude.

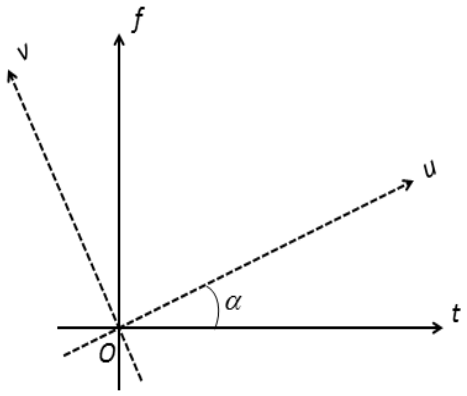

Figure 17.3: Illustration of rotation in the time-frequency domain through FrFT.

Several techniques have been developed to estimate PPS parameters. Commonly used parametric methods estimate the IF through polynomial phase transform, Hough transform, and high-order ambiguity function (HAF) [15, 18, 51].

The HAF is defined as the Fourier transform of the high-order instantaneous moment (HIM) which is given, for a signal $s(t)$, by the following relation:

$$\mathrm{HIM}_K[s(t);\tau] = \prod_{q=0}^{K-1} \left[s^{(*q)}(t - q\tau) \right]^{\binom{K-1}{q}}, \tag{17.10}$$

where K is the HIM order, τ is the lag, and $(\cdot)^{(*q)}$ is an operator defined as

$$s^{(*q)}(t) = \begin{cases} s(t), & \text{if } q \text{ is even,} \\ s^*(t), & \text{if } q \text{ is odd,} \end{cases} \tag{17.11}$$

The Nth order HIM of a PPS given in (17.9) is reduced to a constant amplitude harmonic [35, 50]

$$\mathrm{HIM}_N[s(t);\tau] = A^{2^{N-1}} e^{j(\tilde{\omega}_N t + \tilde{\phi}_N)}, \tag{17.12}$$

where

$$\tilde{\omega}_N = N!\tau^{N-1} a_N, \quad \tilde{\phi}_N = (N-1)!\tau^{N-1} a_{N-1} - 0.5N!(N-1)\tau^N a_N. \tag{17.13}$$

A natural way to take advantage of this property is to compute the Fourier transform of the Nth-order HIM, which leads to the HAF definition:

$$\mathrm{HAF}_N[s;\omega,\tau] = \int_{-\infty}^{\infty} \mathrm{HIM}_N[s(t);\tau] e^{-j\omega t} dt. \tag{17.14}$$

The Nth order polynomial coefficient can be estimated via

$$\hat{a}_N = \frac{1}{N!\tau^{N-1}} \arg\max_{\omega} \{ |\mathrm{HAF}_N(s;\omega,\tau)| \}. \tag{17.15}$$

Using this estimate, the effect of the phase term of the Nth order can be removed:

$$s^{(N-1)}(t) = s(t)e^{-j\hat{a}_N t^N}. \tag{17.16}$$

This process can be repeated to obtain lower order coefficients.

It was pointed out in [16, 50] that the classical procedure for polynomial phase modeling based on HAF method is challenged by the noise robustness and the cross-terms presence. To overcome these problems, the multilag HAF (mlHAF) concept, which is a generalization of the HIM, was proposed in [16]. Consider that the Kth-order HIM as the 2nd-order HIM of the $(K-1)$th-order HIM,

$$\mathrm{HIM}_K(s(t);\tau] = \mathrm{HIM}_2[\mathrm{HIM}_{K-1}[s(t);\tau];\tau]. \tag{17.17}$$

In mlHAF based technique, the HIM is replaced by the multilag HIM (mlHIM), which is expressed as

$$\mathrm{mlHIM}_K(s(t);\boldsymbol{\tau}_{K-1}] = \mathrm{mlHIM}_{K-1}[s(t+\tau_{K-1});\boldsymbol{\tau}_{K-2}] \times \mathrm{mlHIM}^*_{K-1}[s(t-\tau_{K-1});\boldsymbol{\tau}_{K-2}], \tag{17.18}$$

where $\boldsymbol{\tau}_N = [\tau_1, \tau_2, ..., \tau_K]$ is the set of lags. The mlHAF is defined as the Fourier transform of mlHIM in a manner similar to HAF. The performance of HAF-based parameter estimation of multi-component PPS signals are provided in, e.g., [52].

When a nonstationary signal, which is characterized by its IF, is considered over a substantial time period, it may become difficult to use a PPS to model the entire waveform. Rather, it is more practical to partition the waveform into multiple segments, each represents a PPS signal. The segments can be nonoverlapping or partially overlapping. The PPS coefficients are estimated over each segment and then merged together to achieve the global phase behavior of the entire FM signal [27, 35–37]. In this case, multiple PPS parameter estimates can be made in each segment, and the phase continuity over neighboring segments can be utilized as additional constraint for the selection of the most likely parameter set [27, 35].

17.3 Spatial Time-Frequency Distribution

In this section, we first introduce the concept of STFD. Analysis of the subspace estimates based on STFD matrices is then provided. The robustness of these estimates compared to those corresponding to the covariance matrices is the main motivation of using the STFD platform for direction finding of nonstationary signals.

17.3.1 Spatial Time-Frequency Distribution

Consider n narrowband nonstationary signals impinging on an array consisting of m sensors. By *narrowband* signals, we mean that the steering vector does not change with frequency within the signal bandwidth. For simplicity, we assume a 1-D DOA estimation problem (e.g., only the azimuth angle is considered), but the extension to a 2-D problem (i.e., both the azimuth and elevation angles are considered) is straightforward. The $m \times 1$ received data vector $\mathbf{x}(t)$ and the $n \times 1$ source signal vector $\mathbf{d}(t)$ are related by

$$\mathbf{x}(t) = \mathbf{A}(\boldsymbol{\theta})\mathbf{d}(t) + \mathbf{n}(t), \tag{17.19}$$

where $\mathbf{A}(\boldsymbol{\theta}) = [\mathbf{a}(\theta_1), \mathbf{a}(\theta_2), ..., \mathbf{a}(\theta_n)]$ is the $m \times n$ mixing matrix that holds the steering vectors of the n signals, $\boldsymbol{\theta} = [\theta_1, \theta_2, ..., \theta_n]$, and $\mathbf{a}(\theta_q)$ is the steering vector for the qth source, who signal $d_q(t)$ arrives from direction θ_q. Each element of $\mathbf{d}(t) = [d_1(t), d_2(t), ..., d_n(t)]^T$ is assumed to be a mono-component signal. Due

to the signal mixing occurring at each sensor, the elements of $\mathbf{x}(t)$ become multi-component signals. $\mathbf{n}(t)$ is an $m \times 1$ additive noise vector that consists of independent and identically distributed (i.i.d.) zero-mean, white and complex Gaussian distributed processes with variance σ_n^2. The noise elements are assumed to be independent of the signals, which are assumed to be deterministic.

The STFD matrix of vector $\mathbf{x}(t)$ is expressed as [12]

$$\mathbf{D}_{\mathbf{xx}}(t,f) = \int_{-\infty}^{\infty}\int_{-\infty}^{\infty} \phi(t-u,\tau)\mathbf{x}\left(u+\frac{\tau}{2}\right)\mathbf{x}^H\left(u-\frac{\tau}{2}\right)e^{-j2\pi f\tau}dud\tau, \tag{17.20}$$

where the (i,k)th element of $\mathbf{D}_{\mathbf{xx}}(t,f)$ is given in (17.2) for $i,k = 1,2,...,m$. The noise-free STFD matrix is obtained by substituting (17.19) into (17.20), resulting in

$$\mathbf{D}_{\mathbf{xx}}(t,f) = \mathbf{A}(\boldsymbol{\theta})\mathbf{D}_{\mathbf{dd}}(t,f)\mathbf{A}^H(\boldsymbol{\theta}) \tag{17.21}$$

where $\mathbf{D}_{\mathbf{dd}}(t,f)$ is the TFD matrix of $\mathbf{d}(t)$ which consists of auto-source TFDs as its diagonal elements and cross-source TFDs as its off-diagonal elements. With the presence of noise, the expected value of $\mathbf{D}_{\mathbf{xx}}(t,f)$ becomes

$$\mathrm{E}[\mathbf{D}_{\mathbf{xx}}(t,f)] = \mathbf{A}(\boldsymbol{\theta})\mathbf{D}_{\mathbf{dd}}(t,f)\mathbf{A}^H(\boldsymbol{\theta}) + \sigma_n^2\mathbf{I}_m. \tag{17.22}$$

Equation (17.22) relates the STFD matrix to the source TFD matrix in a manner similar to the formula that is commonly used in narrowband array processing problems, relating the source covariance matrix to the sensor spatial covariance matrix. It is clear, therefore, that the two subspaces spanned by the principle eigenvectors of $\mathbf{D}_{\mathbf{xx}}(t,f)$ and the columns of $\mathbf{A}(\boldsymbol{\theta})$ are identical. As discussed below, the construction of the STFD matrix from the t-f points of highly localized signal energy allows the corresponding signal and noise subspace estimates to become more robust to noise than their counterparts obtained using the data covariance matrix [12, 75]. Further, source elimination, rendered through the selection of specific t-f regions, improves DOA estimations [75].

17.3.2 SNR Enhancement

To provide insights into the properties of STFDs, we consider the case of frequency modulated (FM) signals and the simplest form of TFD, namely, the pseudo Wigner-Ville distribution (PWVD) [75]. The consideration of FM signals is motivated by the fact that these signals are uniquely characterized by their IFs, and therefore, they have clear t-f signatures that can be utilized by the STFD approach. Also, FM the signals have constant amplitudes. The FM signals can be modeled as

$$\mathbf{d}(t) = [d_1(t),...,d_n(t)]^T = [D_1e^{j\psi_1(t)},...,D_ne^{j\psi_n(t)}]^T, \tag{17.23}$$

where D_i and $\psi_i(t)$ are the fixed amplitude and time-varying phase of ith source signal. For each sampling time t, $d_i(t)$ has an IF of $f_i(t) = d\psi_i(t)/(2\pi dt)$. For the simplicity of the analysis, we further assume that the third-order derivative of the phase is negligible over the window length L.

The discrete form of PWVD of a signal $x(t)$, using a rectangular window of odd length L, is given by

$$D_{xx}(t,f) = \sum_{\tau=-(L-1)/2}^{(L-1)/2} x(t+\tau)x^*(t-\tau)e^{-j4\pi f\tau}. \tag{17.24}$$

Similarly, the spatial pseudo Wigner-Ville distribution (SPWVD) matrix is obtained as

$$\mathbf{D}_{\mathbf{xx}}(t,f) = \sum_{\tau=-(L-1)/2}^{(L-1)/2} \mathbf{x}(t+\tau)\mathbf{x}^H(t-\tau)e^{-j4\pi f\tau}. \tag{17.25}$$

The ith diagonal element of PWVD matrix $\mathbf{D_{dd}}(t, f)$ is given by

$$D_{d_i d_i}(t, f) = \sum_{\tau=-(L-1)/2}^{(L-1)/2} D_i^2 e^{j[\psi_i(t+\tau)-\psi_i(t-\tau)]-j4\pi f\tau}. \tag{17.26}$$

Assume that the third-order derivative of the phase is negligible over the window length L, then along the true t-f points of the ith signal, $f_i(t) = d\psi_i(t)/(2\pi dt)$, and $\psi_i(t+\tau) - \psi_i(t-\tau) - 4\pi f_i(t)\tau = 0$. Accordingly, for $(L-1)/2 \le t \le N - (L-1)/2$,

$$D_{d_i d_i}(t, f_i(t)) = \sum_{\tau=-(L-1)/2}^{(L-1)/2} D_i^2 = LD_i^2. \tag{17.27}$$

Similarly, the noise SPWVD matrix $\mathbf{D_{nn}}(t, f)$ is

$$\mathbf{D_{nn}}(t, f) = \sum_{\tau=-(L-1)/2}^{(L-1)/2} \mathbf{n}(t+\tau)\mathbf{n}^H(t-\tau)e^{-j4\pi f\tau}, \tag{17.28}$$

whose statistical expectation is $\mathrm{E}\left[\mathbf{D_{nn}}(t, f)\right] = \sigma_n^2\mathbf{I}_m$. Therefore, when we select the t-f points along the t-f signature or the IF of the ith FM signal, the SNR in the STFD matrix $\mathrm{E}[\mathbf{D_{xx}}(t, f)]$ becomes LD_i^2/σ_n^2, which has an improved factor L over the covariance matrix $\mathbf{R_{xx}} = \mathrm{E}[\mathbf{x}(t)\mathbf{x}^H(t)]$.

The PWVD of each FM source has a constant value over the observation period, providing that we leave out the rising and falling power distributions at both ends of the data record. For convenience, we select those $N' = N - L + 1$ t-f points of constant distribution value for each source signal. In the case where the STFD matrices are averaged over the t-f signatures of n_o sources, i.e., a total of $n_o N'$ t-f points, the result is given by

$$\hat{\mathbf{D}} = \frac{1}{n_o N'} \sum_{q=1}^{n_o} \sum_{i=1}^{N'} \mathbf{D_{xx}}(t_i, f_{q,i}(t_i)), \tag{17.29}$$

where $f_{q,i}(t_i)$ is the IF of the qth signal at the ith time sample. The expectation of the averaged STFD matrix is

$$\mathbf{D} = \frac{1}{n_o} \sum_{q=1}^{n_o} \left[LD_q^2 \mathbf{a}_q \mathbf{a}_q^H + \sigma_n^2\mathbf{I}\right] = \frac{L}{n_o}\mathbf{A}^o\mathbf{R}_{\mathbf{dd}}^o(\mathbf{A}^o)^H + \sigma_n^2\mathbf{I}, \tag{17.30}$$

where $\mathbf{R}_{\mathbf{dd}}^o = \mathrm{Diag}\left[D_i^2, i = 1, 2, \cdots, n_o\right]$ and $\mathbf{A}^o = \left[\mathbf{a}_1, \mathbf{a}_2, \cdots, \mathbf{a}_{n_o}\right]$ represent the signal correlation matrix and the mixing matrix formulated by considering n_o signals out of the total number of n signal arrivals, respectively.

It is clear from (17.30) that the SNR improvement $G = L/n_o$ (we assume $L > n_o$) is inversely proportional to the number of sources contributing to matrix $\mathbf{D}$. Therefore, from the SNR perspective, it is best to set $n_o = 1$, i.e., to select the sets of N' t-f points that belong to individual signals one set at a time, and then separately evaluate the respective STFD matrices.

This procedure is made possible by the fact that STFD-based array processing is, in essence, a discriminatory technique in the sense that it does not require simultaneous localization and extraction of all unknown signals received by the array. Array processing can be performed using STFDs of a subclass of the impinging signals with specific t-f signatures. In this respect, the t-f based direction finding techniques

have implicit spatial filtering, removing the undesired signals from consideration. It is also important to note that with the ability to construct the STFD matrix from one or few signal arrivals, the well known $m > n$ condition on source localization using arrays can be relaxed to $m > n_o$, i.e., we can perform direction finding or source separation with the number of array sensors smaller than the number of impinging signals. Further, from the angular resolution perspective, closely spaced sources with different t-f signatures can be resolved by constructing two separate STFDs, each corresponding to one source, and then proceed with subspace decomposition for each STFD matrix, followed by an appropriate source localization method (MUSIC, for example). The drawback using different STFD matrices separately is of course the need for repeated computations. Relevant work for noise analysis and SNR enhancement in the t-f domain can be found in [2, 32, 60, 61].

17.3.3 Subspace Analysis

Analysis of the eigendecomposition of the STFD matrix is closely related to the analysis of subspace decomposition of the covariance matrix [58]. Before elaborating on this relationship, we present the case of FM signals using the conventional covariance matrix approach.

In equation (17.19), it is assumed that the number of sensors is greater than the number of sources, i.e., $m > n$. Further, matrix $\mathbf{A}$ is full column rank. We further assume that the correlation matrix $\mathbf{R_{xx}} = \mathrm{E}[\mathbf{x}(t)\mathbf{x}^H(t)]$ is nonsingular, and the observation period consists of N snapshots with $N > m$. Under the above assumptions, the correlation matrix is given by

$$\mathbf{R_{xx}} = \mathrm{E}[\mathbf{x}(t)\mathbf{x}^H(t)] = \mathbf{A}\mathbf{R_{dd}}\mathbf{A}^H + \sigma_n^2\mathbf{I}_m, \tag{17.31}$$

where $\mathbf{R_{dd}} = \mathrm{E}[\mathbf{d}(t)\mathbf{d}^H(t)]$ is the source correlation matrix.

Let $\lambda_1 > \lambda_2 > \cdots > \lambda_n > \lambda_{n+1} = \lambda_{n+2} = \cdots = \lambda_m = \sigma_n^2$ denote the eigenvalues of $\mathbf{R_{xx}}$. It is assumed that λ_i, $i = 1, \cdots, n$, are distinct. The unit-norm eigenvectors associated with $\lambda_1, ..., \lambda_n$ constitute the columns of matrix $\mathbf{S} = [\mathbf{s}_1, ..., \mathbf{s}_n]$ that spans the signal subspace, and those corresponding to $\lambda_{n+1}, ..., \lambda_m$ make up matrix $\mathbf{G} = [\mathbf{g}_1, ..., \mathbf{g}_{m-n}]$ that spans the noise subspace. Since the columns of $\mathbf{A}$ and $\mathbf{S}$ span the same subspace, then $\mathbf{A}^H\mathbf{G} = \mathbf{0}$.

In practice, $\mathbf{R_{xx}}$ is unknown, and therefore should be estimated from the available data samples (snapshots) $\mathbf{x}(i)$, $i = 1, 2, ..., N$. The estimated correlation matrix is given by $\hat{\mathbf{R}}_{\mathbf{xx}} = \frac{1}{N}\sum_{i=1}^{N}\mathbf{x}(i)\mathbf{x}^H(i)$. Let $\{\hat{\mathbf{s}}_1, ..., \hat{\mathbf{s}}_n, \hat{\mathbf{g}}_1, ..., \hat{\mathbf{g}}_{m-n}\}$ denote the unit-norm eigenvectors of $\hat{\mathbf{R}}_{\mathbf{xx}}$, arranged in the descending order of the associated eigenvalues, and let $\hat{\mathbf{S}} = [\hat{\mathbf{s}}_1, ..., \hat{\mathbf{s}}_n]$ and $\hat{\mathbf{G}} = [\hat{\mathbf{g}}_1, ..., \hat{\mathbf{g}}_{m-n}]$.

We assume that the transmitted signals propagate in a stationary environment and are mutually uncorrelated over the observation period $1 \le t \le N$, i.e., $\frac{1}{N}\sum_{k=1}^{N} d_i(k)d_l^*(k) = 0$, for $i \neq l$, $i, l = 1, ..., n$. In this case, the signal correlation matrix is

$$\mathbf{R_{dd}} = \lim_{T\to\infty}\frac{1}{T}\sum_{t=1}^{T}\mathbf{d}(t)\mathbf{d}^H(t) = \mathrm{Diag}\left[D_1^2, ..., D_n^2\right]. \tag{17.32}$$

Lemma 1 [75]: For uncorrelated FM signals with additive white Gaussian noise, the orthogonal projections of $\{\hat{\mathbf{g}}_i\}$ onto the column space of $\mathbf{S}$ are asymptotically (for large N) jointly Gaussian distributed with zero means and covariance matrices given by

$$E\left[\left(\mathbf{S}\mathbf{S}^H\hat{\mathbf{g}}_i\right)\left(\mathbf{S}\mathbf{S}^H\hat{\mathbf{g}}_j\right)^H\right] = \frac{\sigma_n^2}{N}\left[\sum_{k=1}^{n}\frac{\lambda_k}{(\sigma_n^2 - \lambda_k)^2}\mathbf{s}_k\mathbf{s}_k^H\right]\delta_{i,j} \triangleq \frac{1}{N}\mathbf{U}\delta_{i,j}, \tag{17.33}$$

$$E\left[\left(\mathbf{S}\mathbf{S}^H\hat{\mathbf{g}}_i\right)\left(\mathbf{S}\mathbf{S}^H\hat{\mathbf{g}}_j\right)^T\right] = 0 \text{ for all } i,\ j. \tag{17.34}$$

The following Lemma provides the relationship between the eigendecompositions of the STFD matrices and the data covariance matrices used in conventional array processing.

Lemma 2 [75]: Let $\lambda_1^o > \lambda_2^o > \cdots > \lambda_{n_o}^o > \lambda_{n_o+1}^o = \lambda_{n_o+2}^o = \cdots = \lambda_m^o = \sigma_n^2$ denote the eigenvalues of $\mathbf{R}_{\mathbf{xx}}^o = \mathbf{A}^o\mathbf{R}_{\mathbf{dd}}^o(\mathbf{A}^o)^H + \sigma_n^2\mathbf{I}_m$, which is defined from a data record of a mixture of the n_o selected FM signals. Denote the unit-norm eigenvectors associated with $\lambda_1^o, ..., \lambda_{n_o}^o$ by the columns of $\mathbf{S}^o = [\mathbf{s}_1^o, ..., \mathbf{s}_{n_o}^o]$, and those corresponding to $\lambda_{n_o+1}^o, ..., \lambda_m^o$ by the columns of $\mathbf{G}^o = [\mathbf{g}_1^o, ..., \mathbf{g}_{m-n_o}^o]$. We also denote $\lambda_1^{tf} > \lambda_2^{tf} > \cdots > \lambda_{n_o}^{tf} > \lambda_{n_o+1}^{tf} = \lambda_{n_o+2}^{tf} = \cdots = \lambda_m^{tf} = (\sigma_n^{tf})^2$ as the eigenvalues of $\mathbf{D}$ defined in (17.30). The superscript ^{tf} denotes that the associated term is derived from the STFD matrix $\mathbf{D}$. The unit-norm eigenvectors associated with $\lambda_1^{tf}, ..., \lambda_{n_o}^{tf}$ are represented by the columns of $\mathbf{S}^{tf} = [\mathbf{s}_1^{tf}, ..., \mathbf{s}_{n_o}^{tf}]$, and those corresponding to $\lambda_{n_o+1}^{tf}, ..., \lambda_m^{tf}$ are represented by the columns of $\mathbf{G}^{tf} = [\mathbf{g}_1^{tf}, ..., \mathbf{g}_{m-n_o}^{tf}]$. Then,

a) The signal and noise subspaces of $\mathbf{S}^{tf}$ and $\mathbf{G}^{tf}$ are the same as $\mathbf{S}^o$ and $\mathbf{G}^o$, respectively.

b) The eigenvalues have the following relationship:

$$\lambda_i^{tf} = \begin{cases} \dfrac{L}{n_o}\left(\lambda_i^o - \sigma_n^2\right) + \sigma_n^2 = \dfrac{L}{n_o}\lambda_i^o + \left(1 - \dfrac{L}{n_o}\right)\sigma_n^2, & i \le n_o, \\ (\sigma_n^{tf})^2 = \sigma_n^2, & n_o < i \le m. \end{cases} \tag{17.35}$$

An important conclusion from Lemma 2 is that, the largest n_o eigenvalues are amplified using STFD analysis. This improves detection of the number of the impinging signals on the array, as it widens the separation between dominant and noise-level eigenvalues. Determination of the number of signals is key to establishing the proper signal and noise subspaces, and subsequently plays a fundamental role in subspace-based applications. When the input SNR is low, or the signals are closely spaced, the number of signals may often be underdetermined. When the STFD is applied, the SNR threshold level and/or angle separation necessary for the correct determination of the number of signals are greatly reduced.

Next we consider the signal and noise subspace estimates from a finite number of data samples. We form the STFD matrix based on the true (t, f) points along the IF of the n_o FM signals.

Lemma 3 [74, 75]: If the third-order derivative of the phase of the FM signals is negligible over the time-period $[t - L + 1, t + L - 1]$, then the orthogonal projections of $\left\{\hat{\mathbf{g}}_i^{tf}\right\}$ onto the column space of $\mathbf{S}^{tf}$ are asymptotically (for $N \gg L$) jointly Gaussian distributed with zero means and covariance matrices given by

$$\begin{aligned} E\left(\mathbf{S}^{tf}\left(\mathbf{S}^{tf}\right)^H\hat{\mathbf{g}}_i^{tf}\right)\left(\mathbf{S}^{tf}\left(\mathbf{S}^{tf}\right)^H\hat{\mathbf{g}}_j^{tf}\right)^H &= \frac{\sigma_n^2 L}{n_o N'}\left[\sum_{k=1}^{n_o}\frac{\lambda_k^{tf}}{(\sigma_n^2 - \lambda_k^{tf})^2}\mathbf{s}_k^{tf}\left(\mathbf{s}_k^{tf}\right)^H\right]\delta_{i,j} \\ &= \frac{\sigma_n^2}{N'}\left[\sum_{k=1}^{n_o}\frac{(\lambda_k^o - \sigma_n^2) + \frac{n_o}{L}\sigma_n^2}{(\sigma_n^2 - \lambda_k^o)^2}\mathbf{s}_k^o\left(\mathbf{s}_k^o\right)^H\right]\delta_{i,j} \triangleq \frac{1}{N'}\mathbf{U}^{tf}\delta_{i,j}, \end{aligned} \tag{17.36}$$

$$E\left(\mathbf{S}^{tf}\left(\mathbf{S}^{tf}\right)^H\hat{\mathbf{g}}_i^{tf}\right)\left(\mathbf{S}^{tf}\left(\mathbf{S}^{tf}\right)^H\hat{\mathbf{g}}_j^{tf}\right)^T = \mathbf{0} \text{ for all } i,\ j. \tag{17.37}$$

From (17.36) and (17.37), two important observations are in order. First, if the signals are both localizable and separable in the t-f domain, then the reduction of the number of signals from n to n_o greatly reduces the estimation error, specifically when the signals are closely spaced. The second observation relates to SNR enhancements. The above equations show that error reductions using STFDs are more pronounced for the cases of low SNR and/or closely spaced signals. It is clear from (17.36) and (17.37) that, when $\lambda_k^o \gg \sigma_n^2$ for all $k = 1, 2, ..., n_o$, the results are almost independent of L (suppose $N \gg L$ so that $N' = N - L + 1 \simeq N$), and

therefore there would be no obvious improvement in using the STFD over conventional array processing. On the other hand, when some of the eigenvalues are close to σ_n^2 ($\lambda_k^o \simeq \sigma_n^2$, for some $k = 1, 2, ..., n_o$), which is the case of weak or closely spaced signals, all the results of above three equations are reduced by a factor of up to $G = L/n_o$, respectively. This factor represents, in essence, the gain achieved from using STFD processing.

17.4 DOA Estimation Techniques

In this section, we first introduce the STFD-based DOA estimation techniques under the narrowband signal model. T-f MUSIC and t-f maximum likelihood (ML) are used as examples. These techniques demonstrate the advantages of the STFD framework, as described in the previous section. The t-f MUSIC is relatively simple, whereas t-f ML is more computationally demanding, but allows high-resolution DOA estimation of coherent signals. We address the effect of t-f cross-terms on direction finding performance. We then introduce the DOA estimation techniques based on parametric models of nonstationary signals. Depending on the characteristics of the nonstationary signals, different techniques can be used. Fractional transform is discussed for LFM signals, whereas techniques based on signal stationarization allows high-resolution DOA estimations of higher-order polynomial phase signals. DOA estimation based on spatial joint-variable domain distributions, such as the spatial ambiguity function (SAF), is also introduced. Finally, STFD-based DOA estimation of wideband signals is discussed.

17.4.1 Time-Frequency MUSIC

Without loss of generality, we consider 1-D direction finding where the DOAs are described by θ. First, recall that the DOAs are estimated in the MUSIC technique by determining the n values of θ for which the following spatial spectrum is maximized [57],

$$f_{\mathrm{MU}}(\theta) = \left[\mathbf{a}^H(\theta)\hat{\mathbf{G}}\hat{\mathbf{G}}^H\mathbf{a}(\theta)\right]^{-1} = \left[\mathbf{a}^H(\theta)\left(\mathbf{I} - \hat{\mathbf{S}}\hat{\mathbf{S}}^H\right)\mathbf{a}(\theta)\right]^{-1}, \tag{17.38}$$

where $\mathbf{a}(\theta)$ is the steering vector corresponds to θ. The variance of those estimates in the MUSIC technique, assuming white noise processes, is given by [58]

$$\mathrm{E}\left(\hat{\omega}_i - \omega_i\right)^2 = \frac{1}{2N}\frac{\mathbf{a}^H(\theta_i)\mathbf{U}\mathbf{a}(\theta_i)}{h(\theta_i)} \tag{17.39}$$

where $\omega_i = (2\pi d/\lambda)\sin\theta_i$ is the spatial frequency associated with DOA θ_i, d is the interelement spacing, and λ is the wavelength. $\hat{\omega}_i$ is the estimate of ω obtained from the MUSIC. Moreover, $\mathbf{U}$ is defined in (17.33), and

$$h(\theta_i) = \mathbf{d}^H(\theta_i)\mathbf{G}\mathbf{G}^H\mathbf{d}(\theta_i), \quad \text{with} \quad \mathbf{d}(\theta_i) = d\mathbf{a}(\theta_i)/d\omega. \tag{17.40}$$

Similarly, for t-f MUSIC with n_o signals selected, the DOAs are determined by locating the n_o peaks of the spatial spectrum defined from the n_o signals' t-f regions,

$$f_{\mathrm{MU}}^{tf}(\theta) = \left[\mathbf{a}^H(\theta)\hat{\mathbf{G}}^{tf}\left(\hat{\mathbf{G}}^{tf}\right)^H\mathbf{a}(\theta)\right]^{-1} = \left[\mathbf{a}^H(\theta)\left(\mathbf{I} - \hat{\mathbf{S}}^{tf}\left(\hat{\mathbf{S}}^{tf}\right)^H\right)\mathbf{a}(\theta)\right]^{-1}. \tag{17.41}$$

$\hat{\mathbf{G}}^{tf}$ and $\hat{\mathbf{S}}^{tf}$ can be obtained by using either joint block diagonalization (JBD) [13] or t-f averaging. When the t-f averaging is used, the variance of the DOA estimates based on t-f MUSIC is obtained, from the results

of Lemmas 2 and 3, as [75],

$$E\left(\hat{\omega}_i^{tf} - \omega_i\right)^2 = \frac{1}{2N'} \frac{\mathbf{a}^H(\theta_i)\mathbf{U}^{tf}\mathbf{a}(\theta_i)}{h^{tf}(\theta_i)} \tag{17.42}$$

where $\hat{\omega}_i^{tf}$ is the estimate of ω_i, $\mathbf{U}^{tf}$ is defined in (17.36), and

$$h^{tf}(\theta_i) = \mathbf{d}^H(\theta_i)\mathbf{G}^{tf}\left(\mathbf{G}^{tf}\right)^H\mathbf{d}(\theta_i). \tag{17.43}$$

Note that $h^{tf}(\theta) = h(\theta_i)$ if $n_o = n$.

Examples

Consider a uniform linear array of 8 sensors spaced by half a wavelength, and an observation period of 1024 samples. Two chirp signals emitted from two sources positioned at angles θ_1 and θ_2. The start and end frequencies of the signal source at θ_1 are $\omega_{s1} = 0$ and $\omega_{e1} = \pi$, while the corresponding two frequencies for the other source at θ_2 are $\omega_{s2} = \pi$ and $\omega_{e2} = 0$, respectively.

Figure 17.4 displays the variance of the estimated DOA $\hat{\theta}_1$ versus SNR for the case $(\theta_1, \theta_2) = (-10^\circ, 10^\circ)$. The curves in this figure show the theoretical and simulation results of the conventional MUSIC and t-f MUSIC (for L=33 and 129). The Cramer-Rao bound (CRB) is also shown in Figure 17.4 for comparison. Both signals were selected when performing t-f MUSIC ($n_o = n = 2$). Simulation results were averaged over 100 independent Monte-Carlo runs. The advantages of t-f MUSIC in low SNR cases are evident from this figure. The simulation results deviate from the theoretical results for low SNR. This is due to considering only the lowest coefficient order of the perturbation expansion in deriving the theoretical results [75]. Figure 17.5 shows estimated spatial spectra at SNR=−20 dB based on t-f MUSIC ($L = 129$) and the conventional MUSIC. The t-f MUSIC spectral peaks are clearly resolved.

Figure 17.6 shows examples of the estimated spatial spectrum based on t-f MUSIC ($L = 129$) and the conventional MUSIC where the angle separation is small ($\theta_1 = -2.5^o$, $\theta_2 = 2.5^o$). The input SNR is −5 dB. Two t-f MUSIC algorithms are performed using two sets of t-f points, each set belongs to the t-f signature of one source ($n_o = 1$). It is evident that the two signals cannot be resolved when the conventional MUSIC is applied, whereas by utilizing the signals' distinct t-f signatures and applying t-f MUSIC separately for each signal, the two signals become clearly separated and a reasonable DOA estimation is achieved. It is noted that there is a small bias in the estimates of t-f MUSIC due to the imperfect separation of the two signals in the t-f domain.

17.4.2 Time-Frequency Maximum Likelihood Method

In this section, we introduce the time-frequency maximum likelihood (t-f ML) method that can deal with coherent nonstationary sources [5, 74]. For conventional ML methods, the joint density function of the sampled data vectors $\mathbf{x}(1), \mathbf{x}(2), ..., \mathbf{x}(N)$, is given by [76]

$$f(\mathbf{x}(1), \ldots, \mathbf{x}(N)) = \prod_{i=1}^{N} \frac{1}{\pi^m \det[\sigma_n^2\mathbf{I}]} \exp\left(-\frac{1}{\sigma_n^2}\left[\mathbf{x}(i) - \mathbf{A}\mathbf{d}(i)\right]^H\left[\mathbf{x}(i) - \mathbf{A}\mathbf{d}(i)\right]\right). \tag{17.44}$$

It follows from (17.44) that the log-likelihood function of the observations $\mathbf{x}(1), \mathbf{x}(2), \ldots, \mathbf{x}(N)$, is given by

$$L = -mN\ln\sigma_n^2 - \frac{1}{\sigma_n^2}\sum_{i=1}^{N}\left[\mathbf{x}(i) - \mathbf{A}\mathbf{d}(i)\right]^H\left[\mathbf{x}(i) - \mathbf{A}\mathbf{d}(i)\right]. \tag{17.45}$$

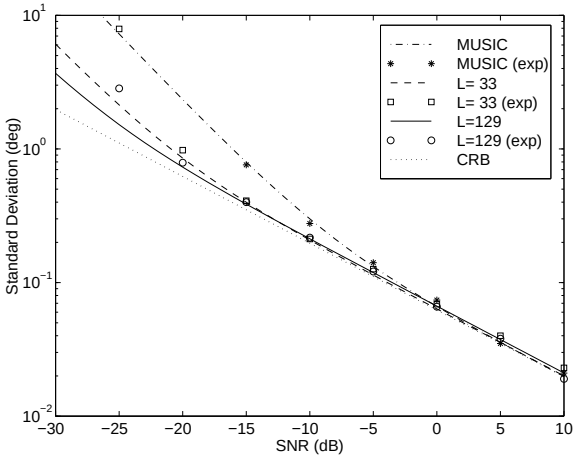

Figure 17.4: Variance of DOA estimation versus input SNR.

To carry out this minimization, we fix $\mathbf{A}$ and minimize (17.45) with respect to $\mathbf{d}$. This yields the well-known solution

$$\hat{\mathbf{d}}(i) = \left[\mathbf{A}^H\mathbf{A}\right]^{-1}\mathbf{A}^H\mathbf{x}(i). \tag{17.46}$$

We can obtain the concentrated likelihood function as [76]

$$F_{\mathrm{ML}}(\theta) = \mathrm{tr}\left\{\left[\mathbf{I}_m - \hat{\mathbf{A}}(\hat{\mathbf{A}}^H\hat{\mathbf{A}})^{-1}\hat{\mathbf{A}}^H\right]\hat{\mathbf{R}}_{\mathbf{xx}}\right\}. \tag{17.47}$$

The ML estimate of θ is obtained as the minimizer of (17.47). Let ω_i and $\hat{\omega}_i$, respectively, denote the spatial frequency and its ML estimate associated with θ_i, then the estimation error $(\hat{\omega}_i - \omega_i)$ are asymptotically (for large N) jointly Gaussian distributed with zero means and the covariance matrix [58]

$$E\left[(\hat{\omega}_i - \omega_i)^2\right] = \frac{1}{2N}\left[\mathrm{Re}(\mathbf{H}\odot\mathbf{R}_{\mathbf{dd}}^T)\right]^{-1}\cdot\mathrm{Re}\left[\mathbf{H}\odot(\mathbf{R}_{\mathbf{dd}}\mathbf{A}^H\mathbf{U}\mathbf{A}\mathbf{R}_{\mathbf{dd}})^T\right]\left[\mathrm{Re}(\mathbf{H}\odot\mathbf{R}_{\mathbf{dd}}^T)\right]^{-1} \tag{17.48}$$

where $\mathbf{U}$ is defined in (17.33). Moreover,

$$\mathbf{H} = \mathbf{C}^H\left[\mathbf{I} - \mathbf{A}(\mathbf{A}^H\mathbf{A})^{-1}\mathbf{A}^H\right]\mathbf{C}, \quad \text{with } \mathbf{C} = d\mathbf{A}/d\omega. \tag{17.49}$$

Next we consider the t-f ML method. As we discussed in the previous section, we select $n_o \le n$ signals in the t-f domain. The concentrated likelihood function defined from the STFD matrix is similar to (17.47) and is obtained by replacing $\hat{\mathbf{R}}_{\mathbf{xx}}$ by $\hat{\mathbf{D}}$,

$$F_{\mathrm{ML}}^{tf}(\theta) = \mathrm{tr}\left\{\left[\mathbf{I} - \hat{\mathbf{A}}^o\left((\hat{\mathbf{A}}^o)^H\hat{\mathbf{A}}^o\right)^{-1}(\hat{\mathbf{A}}^o)^H\right]\hat{\mathbf{D}}\right\}. \tag{17.50}$$

Therefore, the estimation error $(\hat{\omega}_i^{tf} - \omega_i)$ associated with the t-f ML method are asymptotically (for $N \gg L$) jointly Gaussian distributed with zero means and the covariance matrix [74]

$$\begin{aligned}\mathrm{E}\left[\left(\hat{\omega}_i^{tf} - \omega_i\right)^2\right] &= \frac{\sigma_n^2}{2N'}\left[\mathrm{Re}(\mathbf{H}^o\odot\mathbf{D}_{\mathbf{dd}}^T)\right]^{-1}\cdot\mathrm{Re}\left[\mathbf{H}^o\odot\left(\mathbf{D}_{\mathbf{dd}}(\mathbf{A}^o)^H\mathbf{U}^{tf}\mathbf{A}^o\mathbf{D}_{\mathbf{dd}}\right)^T\right]\left[\mathrm{Re}(\mathbf{H}^o\odot\mathbf{D}_{\mathbf{dd}}^T)\right]^{-1} \\ &= \frac{\sigma_n^2}{2N'}\left[\mathrm{Re}\left(\mathbf{H}^o\odot(\mathbf{R}_{\mathbf{dd}}^o)^T\right)\right]^{-1}\cdot\mathrm{Re}\left[\mathbf{H}^o\odot\left(\mathbf{R}_{\mathbf{dd}}^o(\mathbf{A}^o)^H\mathbf{U}^{tf}\mathbf{A}^o\mathbf{R}_{\mathbf{dd}}^o\right)^T\right]\left[\mathrm{Re}\left((\mathbf{H}^o\odot\mathbf{R}_{\mathbf{dd}}^o)^T\right)\right]^{-1},\end{aligned} \tag{17.51}$$

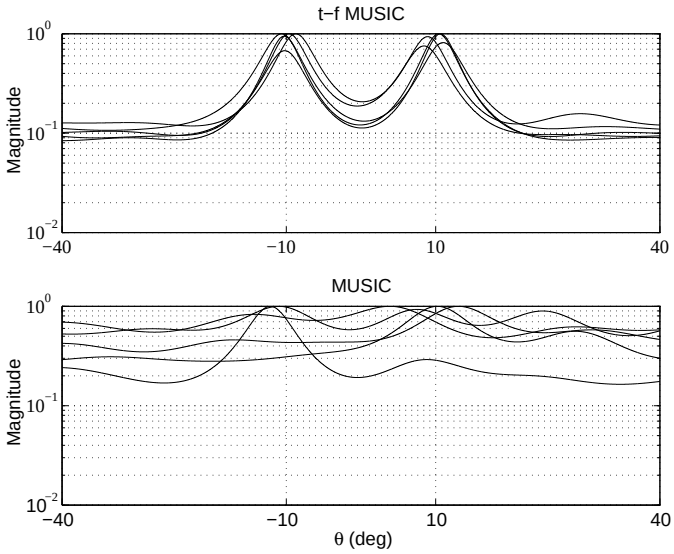

Figure 17.5: Estimated spatial spectra of MUSIC and t-f MUSIC.

where $\mathbf{U}^{tf}$ is defined in (17.36), and

$$\mathbf{H}^o = (\mathbf{C}^o)^H \left[\mathbf{I} - \mathbf{A}^o \left((\mathbf{A}^o)^H \mathbf{A}^o\right)^{-1} (\mathbf{A}^o)^H\right] \mathbf{C}^o, \quad \text{with } \mathbf{C}^o = d\mathbf{A}^o/d\omega. \tag{17.52}$$

In the case of $n_o = n$, then $\mathbf{H}^o = \mathbf{H}$, and $\mathbf{C}^o = \mathbf{C}$.

The signal localization in the t-f domain enables us to select fewer signal arrivals. This fact is not only important in improving the estimation performance, particularly when the signals are closely spaced, but also reduces the dimension of the optimization problem solved by the maximum likelihood algorithm, and subsequently reduces the computational requirement.

Examples

To demonstrate the advantages of t-f ML over both the conventional ML and the t-f MUSIC, consider a uniform linear array of 8 sensors separated by half a wavelength. Two FM signals arrive from $(\theta_1, \theta_2) = (-10^\circ, 10^\circ)$ with the IFs $f_1(t) = 0.2+0.1t/N+0.2\sin(2\pi t/N)$ and $f_2(t) = 0.2+0.1t/N+0.2\sin(2\pi t/N+\pi/2)$, $t = 1, ..., N$. The SNR of both signals is -20 dB, and the number of snapshots used in the simulation is $N = 1024$. We use L=129 for t-f ML. Figure 17.7 shows (θ_1, θ_2) that yield the minimum values of the likelihood function of the t-f ML and the ML methods for 20 independent trials. It is evident that the t-f ML provides much improved DOA estimation over the conventional ML.

In the next example, the t-f ML and the t-f MUSIC are compared for coherent sources. The two coherent FM signals have common IFs $f_{1,2}(t) = 0.2+0.1t/N+0.2\sin(2\pi t/N)$, $t = 1, ..., N$, with a $\pi/2$ phase difference. The signals arrive at $(\theta_1, \theta_2) = (-2^\circ, 2^\circ)$. The SNR of both signals is 5 dB and the number of snapshots is 1024. Figure 17.8 shows the contour plots of the likelihood function of the t-f ML and the estimated spectra of t-f MUSIC for three independent trials. It is clear that the t-f ML can separate the two signals, whereas the t-f MUSIC fails.

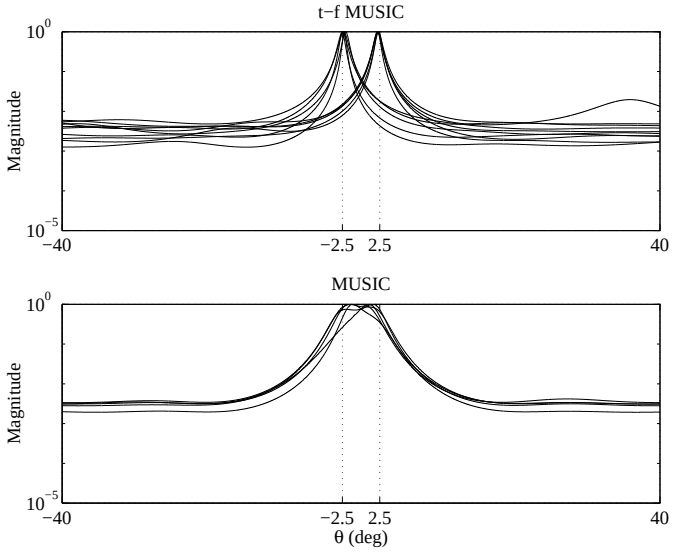

Figure 17.6: Estimated spatial spectra of MUSIC and t-f MUSIC for closely spaced signals.

17.4.3 Effect of Cross-terms

Auto-term and cross-term t-f points have different roles and contribute differently in DOA estimation. This section considers the behavior of cross-terms in DOA estimation and addresses the proper selection of auto-term and cross-term points.

As we discussed in Section 2, cross-terms are a by-product of the TFD due to its bilinearity. Although different kernels have different ways of mitigating cross-terms [23, 39], complete removal of cross-terms, nevertheless, is in general difficult to achieve.

There are two types of cross-terms in the underlying DOA estimation problems. The first type is due to the interactions between the components of the same source signal. These cross-terms always reside, along with the auto-terms, on the main diagonal of the source TFD matrix. This type of cross-terms shares the same steering vector as the auto-terms and thus can be similarly treated. The other type of cross-terms is those generated from the interactions between two signal components belonging to two different sources. These cross-terms are associated with cross-TFD of the source signals and, at any given t-f point, they constitute the off-diagonal entries of the source TFD matrices. Here we consider the second type of cross-terms.

To understand the role of cross-terms in DOA estimation, it is important to compare the cross-terms to the cross-correlation between signals in conventional array processing, whose properties are well studied. The source TFD matrix takes the following general form,

$$\mathbf{D_{dd}}(t,f) = \begin{bmatrix} D_{d_1d_1}(t,f) & D_{d_1d_2}(t,f) & \cdots & D_{d_1d_n}(t,f) \\ D_{d_2d_1}(t,f) & D_{d_2d_2}(t,f) & \cdots & D_{d_2d_n}(t,f) \\ \vdots & \vdots & \ddots & \vdots \\ D_{d_nd_1}(t,f) & D_{d_nd_2}(t,f) & \cdots & D_{d_nd_n}(t,f) \end{bmatrix} \tag{17.53}$$

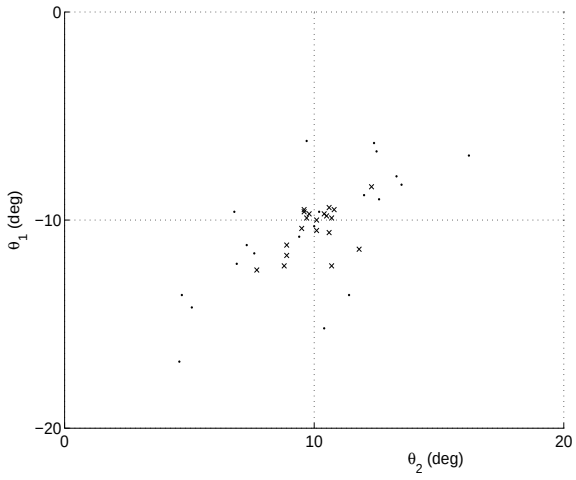

Figure 17.7: (θ_1, θ_2) which minimize the t-f ML ('x') and ML ('·') likelihood functions.

On the other hand, the covariance matrix of correlated source signals is given at the form

$$\mathbf{R_{dd}} = \begin{bmatrix} R_{d_1d_1} & R_{d_1d_2} & \cdots & R_{d_1d_n} \\ R_{d_2d_1} & R_{d_2d_2} & \cdots & R_{d_2d_n} \\ \vdots & \vdots & \ddots & \vdots \\ R_{d_nd_1} & R_{d_nd_2} & \cdots & R_{d_nd_n} \end{bmatrix} \tag{17.54}$$

where the off-diagonal element $R_{d_id_j} = \mathrm{E}[d_i(t)d_j^*(t)]$ represents the correlation between source signals d_i and d_j. Direction finding problems can usually be solved when the signals are partially correlated, however, full rank property of the source covariance matrix $\mathbf{R_{dd}}$ is a necessary condition.

Comparing equations (17.53) and (17.54), it is clear that the cross-correlation terms and the cross-terms have analogous forms. When cross-terms are present at the selected t-f point, these cross-terms appear as off-diagonal elements in the source TFD matrix. On the other hand, when signals are correlated, the off-diagonal elements of the covariance matrix of the source signals represent the cross-correlation between two source signals. DOA estimation problems can usually be solved when the signals are partially correlated, provided that the full rank property of the covariance matrix of the source signals is maintained. The cross-correlation terms and the cross-term TFDs have an analogous form and similar function. That is, cross-term TFDs can be exploited in the DOA estimation as long as the full rank subspace of the STFD matrix is achievable [8]. It is noted that the covariance matrix is obtained as a results of statistical or ensemble averages, whereas the STFD matrix is defined at a (t, f) point and its value usually varies with respect to time t and frequency f. When multiple (t, f) points are incorporated, the effect of a cross-term may be reduced, since the cross-term usually oscillates with respect to time.

17.4.4 DOA Estimation Based on Signal Stationarization

As we discussed in Section 17.2.3, FrFT can "rotate" LFM signals in the t-f domain and become sinusoidal signals in a transformed coordinate system. For narrowband LFM signals, the t-f signatures of the

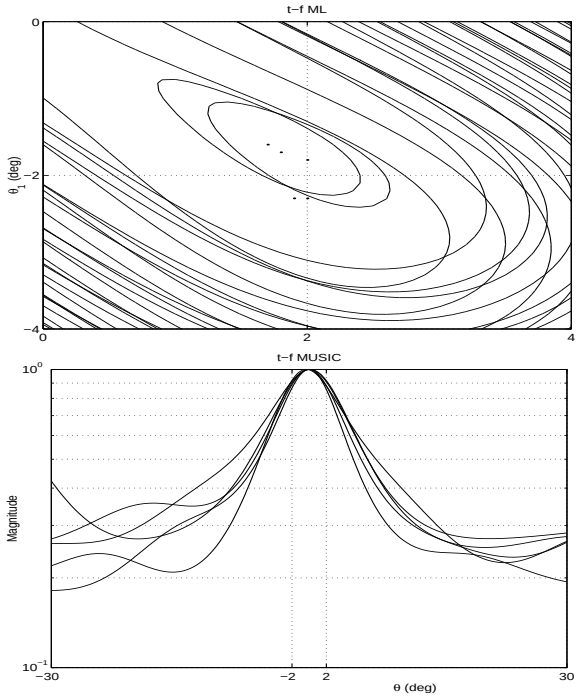

Figure 17.8: Contour plots of t-f ML likelihood function (upper) and spatial spectra of t-f MUSIC (lower).

signals are identical for different array sensors, thus the same rotating operation stationarizes a signal component at all array sensors. Further, mask operations can be applied in the transformed domain to remove the effects of other components, whether they correspond to LFM or nonlinear FM signals. As such, the DOA estimation problem of LFM signals becomes equivalent to that of a single sinusoidal signal [54].

In general, for FM signals that are characterized by PPS or other time-varying IFs, their parameters can be estimated, as discussed in Section 17.2.4. The signal stationarization process converts an FM signal into a sinusoid or DC signal and, as such, allows a similar treatment [36]. The DOA estimation technique based on signal stationarization is proposed in [71].

For receiver array signals

$$\mathbf{x}(t) = \mathbf{A}(\boldsymbol{\theta})\mathbf{d}(t) + \mathbf{n}(t) = \sum_{i=1}^{n} \mathbf{a}_i d_i(t) + \mathbf{n}(t), \tag{17.55}$$

where $d_i(t) = D_i e^{j\phi_i(t)}$, stationarization is performed by multiplying $\mathbf{x}(t)$ with the conjugation of the kth signal component [71],

$$\mathbf{x}^{[k]}(t) = \mathbf{x}(t)e^{-j\phi_k(t)} = \mathbf{a}_k D_k + \sum_{i=1, i\neq k}^{n} \mathbf{a}_i e_i^{j(\phi_i(t)-\phi_k(t))}(t) + \mathbf{n}(t). \tag{17.56}$$

This operation transforms the selected kth signal from an FM signal to a DC signal. Other signal components, shown as the second term at the right-hand side of the above equation, will likely to have nonzero frequencies

whenever the corresponding frequencies satisfy $d\phi_i(t)/dt \neq d\phi_k(t)/dt$ for $i \neq k$. As such, even with some perturbations induced due to imperfect stationarization, a mask around the DC region can be applied to only keep the kth signal, which is subsequently used for DOA estimation.

In [70], the signal stationarization is applied for the direction finding problem of multipath signals in an over-the-horizon radar (OTHR) system. It is shown that the stationarization operation allows separation of multipath signals, which have both closely separated Doppler signatures and close angular separation. This enables DOA estimations of individual components which are otherwise difficult to perform without pre-processing.

17.4.5 DOA Estimation Based on Spatial Joint-Variable Domain Distributions

So far, we have considered the TFD which transforms a 1-D (time-domain) signal into a 2-D representation in the joint t-f domain. It is known that a nonstationary signal can be also represented in other joint-variable domains, such as the joint domain of time-lag and Doppler (frequency-lag), time and time-lag, and frequency and Doppler (frequency-lag) [19].

The ambiguity function of a signal $x(t)$ is defined as

$$B_{xx}(\nu,\tau) = \int_{-\infty}^{\infty} x\left(u+\frac{\tau}{2}\right)x^*\left(u-\frac{\tau}{2}\right)e^{-j\nu\tau}du, \tag{17.57}$$

where ν and τ are the frequency lag and the time lag, respectively.

For the signal observed at an sensor array, we define the spatial ambiguity function (SAF) matrix of a signal vector $\mathbf{x}(t)$ in a similar way to the STFD as [6]

$$\mathbf{B}_{xx}(\nu,\tau) = \int_{-\infty}^{\infty} \mathbf{x}\left(u+\frac{\tau}{2}\right)\mathbf{x}^H\left(u-\frac{\tau}{2}\right)e^{-j\nu\tau}du. \tag{17.58}$$

In a noise-free environment, $\mathbf{x}(t) = \mathbf{A}\mathbf{d}(t)$, the SAF is related to the source ambiguity matrix $\mathbf{B}_{\mathbf{dd}}(\nu,\tau)$ by

$$\mathbf{B}_{\mathbf{xx}}(\nu,\tau) = \mathbf{A}\mathbf{B}_{\mathbf{dd}}(\nu,\tau)\mathbf{A}^H. \tag{17.59}$$

Equations (17.58) and (17.59) are similar to the STFD matrix and thus the SAF inherits the properties of the STFD.

The SAFs have the following two important offerings that distinguish them from other array spatial functions. (1) The cross-terms in between source signals reside on the off-diagonal entries of source ambiguity matrix $\mathbf{B}_{\mathbf{dd}}(\nu,\tau)$. In the ambiguity domain, the signal auto-terms are positioned near and at the origin, making it easier to leave out cross-terms from matrix construction. (2) In the ambiguity domain, the auto-terms of all narrowband signals, regardless of their frequencies and phases, fall on the time-lag axis ($\nu = 0$), while those of the wideband signals fall on a different (ν,τ) region or spread over the entire ambiguity domain. Therefore, the SAF is a natural choice for recovering and spatially localizing narrowband sources in broadband signal platforms.

17.4.6 DOA Estimation of Wideband Nonstationary Signals

The discussion so far has been focused on the DOA estimation of narrowband nonstationary signals. In many applications, the signals are rather wideband. In this case, the DOA estimator should consider the fact that the steering vector is now frequency-dependent.

In order to estimate the DOA for a general class of wideband signals, the conventional techniques usually use Fourier transform to decompose the wideband signals into a set of narrowband components. The narrowband signals can then be processed either incoherently or coherently. The incoherent-based approaches are relatively simple and estimate the DOA from the average of the spatial spectra corresponding to different frequency bins. However, coherent approaches are often preferred due to their superior performance compared to incoherent ones. A popularly used technique, namely, the coherent signal-subspace (CSS) processing technique, was proposed by Wang and Kaveh [64] and was further developed in several papers (see [30] and references therein). The fundamental concept of the CSS techniques is to use a set of focusing matrices that map the steering vector at different frequencies into that at a reference frequency prior to coherent combining.

Several t-f and ambiguity domain based DOA estimation methods have been developed for the estimation of wideband LFM signals [31, 46, 65]. [65] employs the t-f analysis to estimate the chirp rates and compensates the signal chirp structure in an iterative manner. A good estimate of the signal DOAs is required to initialize the iterative processing. By assuming that the wideband signals are separable in the t-f domain and their IFs do not rapidly change, [31] uses a sufficiently short sliding window to construct the STFD matrices so as to preserve the narrowband structure of the array manifold. The focusing matrices are then applied to the STFD matrices at selected t-f points corresponding to the source t-f signatures. [46] considers the ambiguity domain for the DOA estimation of wideband LFM signals whose chirp rates are assumed to be known. Multiple chirps with identical chirp rates are allowed in this technique. Performance of incoherent and coherent processing techniques is also compared in [46].

In essence, STFD framework permits wideband DOA estimation methods incorporating the CSS approaches for nonstationary signals. The nature of the LFM signals and the offering of t-f signal representations may be utilized in several aspects. (i) The decomposition of the LFM signals into a spectrum of frequency bins is inherently performed in the t-f analysis. (ii) For LFM signals that have distinct characteristics in the t-f domain, DOA estimation can be performed on individual sources. (iii) LFM signals are instantaneous narrowband, allowing the focusing matrices to be applied to t-f points.

17.5 Joint DOD/DOA Estimation in MIMO Radar Systems

In this section, we discuss the STFD framework in the context of joint direction-of-departure (DOD)/ direction-of-arrival (DOA) estimation in multiple-input multiple-output (MIMO) radar configurations [69]. MIMO radar is an emerging technology that has attracted much interest in the radar community [29, 43]. By emitting orthogonal waveforms from the transmit array antennas and utilizing matched filterbanks in the receivers to extract the orthogonal waveform components, MIMO radar systems can exploit the spatial diversity and the higher number of degrees of freedom to improve resolution, clutter mitigation, and classification performance. In particular, a monostatic MIMO radar system can provide effective array designs to achieve an extended virtual array, which is the sum coarray of the transmit array and the receive arrays [42, 43]. A bistatic MIMO radar, on the other hand, is capable to jointly estimate the DOD and DOA of targets for enhanced target localization [21, 24, 26, 38]. Bistatic radars, in which the transmitters and receivers are separated by a considerable distance, have received increasing attentions because of many potential advantages, such as detection of stealthy targets, covert receivers for safe operation, and increased coverage [63]. The DOD and DOA information obtained from a bistatic radar system is is particularly important in narrowband radar systems, such as over-the-horizon radar, which do not have a high range resolution [69, 73]. It is shown in [34] that nonstationary processing in a MIMO radar platform also yields improved estimation of motion parameters whose Doppler law is characterized by PPS models.

17.5.1 Signal Model

Consider a bistatic MIMO radar system consisting of N_t closely spaced transmit antennas and N_r closely spaced receive antennas. Denote $\mathbf{S} \in \mathbb{C}^{N_t \times T}$ as the narrowband waveform matrix which contains orthogonal waveforms to be transmitted from N_t antennas over a pulse-repetition period of T fast-time samples. We assume that the waveform orthogonality is achieved in the fast-time domain. That is, by denoting $\mathbf{s}_i$ as the ith row of matrix $\mathbf{S}$, $\mathbf{s}_i$ and $\mathbf{s}_l$ are orthogonal for any $i \neq l$ with different delays, and $\mathbf{s}_i$ is orthogonal to the delayed version of itself. We also assume that $\mathbf{s}_i$ has a unit norm, i.e., $\mathbf{S}\mathbf{S}^H = \mathbf{I}_{N_t}$.

Consider a far-field range cell where L point targets are present with DOD θ_l and DOA ϕ_l, where $l = 1, \cdots, L$. Then, the signal data received at the receive array corresponding to the range cell is expressed as the following $N_r \times 1$ complex vector,

$$\mathbf{X}(t) = \mathbf{A}_r \mathbf{\Gamma}(t) \mathbf{A}_t^H \mathbf{S} + \mathbf{N}(t), \tag{17.60}$$

where t is the slow time index, $\mathbf{A}_r = [\mathbf{a}_r(\phi_1), \cdots, \mathbf{a}_r(\phi_L)]$ and $\mathbf{A}_t = [\mathbf{a}_t(\theta_1), \cdots, \mathbf{a}_t(\theta_L)]$, wih $\mathbf{a}_r(\phi_l) \in \mathbb{C}^{N_r \times 1}$ and $\mathbf{a}_t(\theta_l) \in \mathbb{C}^{N_t \times 1}$ respectively denoting the receive steering vector corresponding to DOA ϕ_l and the transmit steering vector corresponding to DOD θ_l. In addition, $\mathbf{\Gamma}(t) = \text{Diag}[\gamma_1(t), \cdots, \gamma_L(t)]$ where $\gamma_l(t) = \rho_l e^{j2\pi\beta(f_{D,l}(t),t)}$ denotes the complex reflection coefficient of the lth target during the tth pulse repetition period. The complex reflection coefficient is a function of the radar cross section (RCS), represented by ρ_l, and the phase term, denoted as $\beta(f_{D,l}(t), t)$, which depends on the Doppler frequency $f_{D,l}(t)$ of the slow time index t. Moreover, $\mathbf{N}(t) \in \mathbb{C}^{N_r \times T}$ is an additive noise matrix, whose elements are assumed to be i.i.d. complex Gaussian random variables with zero mean and variance σ_n^2. To qualify expression (17.60), it is assumed that the steering vectors remain unchanged during the entire slow-time processing period, which is often the case for far-field targets. The nonstationary signatures result from the maneuvering flights of targets, represented by the Doppler frequency $f_{D,l}(t)$.

By post-multiplying (17.60) by $\mathbf{S}^H$ and utilizing the orthogonality of the transmitted waveforms, we obtain $\mathbf{Y}(t) \in \mathbb{C}^{N_t \times N_r}$ as

$$\mathbf{Y}(t) = \mathbf{A}_r \mathbf{\Gamma}(t) \mathbf{A}_t^H + \mathbf{Z}(t), \tag{17.61}$$

where $\mathbf{Z}(t) = \mathbf{N}(t)\mathbf{S}^H$. Vectorizing $\mathbf{Y}(t)$ in (17.61) yields the following $N_t N_r \times 1$ vector

$$\mathbf{y}(t) = \mathbf{w}(t) + \mathbf{z}(t) = \mathbf{A}\boldsymbol{\gamma}(t) + \mathbf{z}(t), \tag{17.62}$$

where $\mathbf{w}(t) = \mathbf{A}\boldsymbol{\gamma}(t)$ is the noise-free portion of the signal vector,

$$\mathbf{A} = \mathbf{A}_t \diamond \mathbf{A}_r = \left[\mathbf{a}_1^{[t]} \otimes \mathbf{a}_1^{[r]}, ..., \mathbf{a}_L^{[t]} \otimes \mathbf{a}_L^{[r]}\right], \tag{17.63}$$

with $\mathbf{a}_l^{[t]}$ and $\mathbf{a}_l^{[r]}$ denoting the lth column of $\mathbf{A}_t$ and $\mathbf{A}_r$, respectively. In addition, $\boldsymbol{\gamma}(t) = \text{diag}(\mathbf{\Gamma}(t)) = [\gamma_1(t), \cdots, \gamma_L(t)]^T$, and $\mathbf{z}(t) = \text{vec}(\mathbf{Z}(t))$.

The noise component corresponding to the mth transmit waveform and the nth receive antenna is given by $z_{n,m}(t) = [\mathbf{z}(t)]_{(m-1)N_r+n} = \tilde{\mathbf{n}}_n(t)\tilde{\mathbf{s}}_m^H$, where $\tilde{\mathbf{n}}_n(t)$ is the nth row of the receive noise matrix $\mathbf{N}(\mathbf{t})$, and $\tilde{\mathbf{s}}_m$ is the mth row of waveform matrix $\mathbf{S}$, $m = 1, ..., N_t$ and $n = 1, ..., N_r$. Notice that we used $\tilde{(\,)}$ to emphasize a row vector. It is clear that vector $\mathbf{z}(t)$ has a zero mean, spatially white across the virtual sensors, and its covariance matrix can be shown to be $\sigma_n^2 \mathbf{I}_{N_t N_r}$ because

$$\text{E}[z_{n_1,m_1}(t) z_{n_2,m_2}^*(t)] = \text{E}\left[\tilde{\mathbf{n}}_{n_1}(t)\tilde{\mathbf{s}}_{m_1}^H \left(\tilde{\mathbf{n}}_{n_2}(t)\tilde{\mathbf{s}}_{m_2}^H\right)^*\right] = \text{E}[\tilde{\mathbf{s}}_{m_2}\tilde{\mathbf{n}}_{n_2}^H(t)\tilde{\mathbf{n}}_{n_1}(t)\tilde{\mathbf{s}}_{m_1}^H] = \sigma_n^2 \delta_{n1,n2}\delta_{m1,m2}. \tag{17.64}$$

17.5.2 Joint DOD/DOA Estimations

In bistatic radars, the DOD and DOA information can be synthesized to locate targets. For multiple targets, the combination of estimated DOD and DOA yields paring ambiguity. Several techniques have been developed to void or to automatically obtain pairing operation [21, 38]. These approaches, based on ESPRIT [56], or combined ESPRIT-MUSIC, can be extended to the t-f framework. We consider, as an example, the combined ESPRIT-MUSIC technique developed in [21] which only requires two decoupled one-dimensional direction finding operations where the DOD and DOA are automatically paired. In this section, we extend this technique into the STFD framework. The DODs of the targets are first estimated using t-f ESPRIT [33] and their DOAs are then obtained using t-f MUSIC [13]. To apply ESPRIT-based method, both arrays are assumed to be uniform and linear, but the interelement spacings of the two arrays, respectively denoted as d_t and d_r, may differ.

Consider a t-f region Ω_0 that contains signal returns from $L_0 \leq L$ targets. An STFD matrix, denoted as $\mathbf{D}_{\mathbf{yy}}(\Omega_0)$, can be obtained through weighted average of the STFD matrices across region Ω_0, i.e.,

$$\mathbf{D}_{\mathbf{yy}}(\Omega_0) = \sum_{(t,f)\in\Omega_0} w(t,f)\mathbf{D}_{\mathbf{yy}}(t,f), \tag{17.65}$$

where $w(t, f)$ is the weighting coefficients, which can be chosen to be identical or proportional to the TFD magnitude. The signal subspace of matrix $\mathbf{D}_{\mathbf{yy}}(\Omega_0)$ corresponds to the L_0 target signals contained in the selected t-f region Ω_0. In other words, it spans the same subspace as $\mathbf{A}_0$, where $\mathbf{A}_0 = \mathbf{A}_{0,t} \diamond \mathbf{A}_{0,r}$ is a $N_tN_r \times L_0$ submatrix of $\mathbf{A}$ that contains the L_0 columns of matrix $\mathbf{A}$, corresponding to the L_0 signals included in the selected t-f region.

Performing eigendecomposition of $\mathbf{D}_{\mathbf{yy}}(\Omega_0)$ and denote $\mathbf{U}_{s,0}$ as its $N_tN_r \times L_0$ signal subspace, whereas $\mathbf{U}_{n,0}$ as the $N_tN_r \times (N_tN_r - L_0)$ noise subspace. Then, $\mathbf{U}_{s,0}$ and $\mathbf{A}_0$ are related by an unknown transformation matrix $\mathbf{T}$ as

$$\mathbf{U}_{s,0} = \mathbf{A}_0\mathbf{T}. \tag{17.66}$$

Divide the virtual array into two overlapping subarrays, respectively consisting of the first and last $(N_t - 1)N_r$ virtual antennas. Denote $\mathbf{A}_{0,t}^{(1)}$ and $\mathbf{A}_{0,t}^{(2)}$ as the first and last $N_t - 1$ rows of $\mathbf{A}_{0,t}$, and let $\mathbf{A}_0^{(t1)} = \mathbf{A}_{0,t}^{(1)} \diamond \mathbf{A}_{0,r}$ and $\mathbf{A}_0^{(t2)} = \mathbf{A}_{0,t}^{(2)} \diamond \mathbf{A}_{0,r}$. Further, denote the averaged STFD matrices defined in these subarrays as $\mathbf{D}_{\mathbf{yy}}^{(1)}(\Omega_0)$ and $\mathbf{D}_{\mathbf{yy}}^{(2)}(\Omega_0)$, respectively. Then, their respective signal subspaces relate to $\mathbf{A}_0^{(t1)}$ and $\mathbf{A}_0^{(t2)}$ through

$$\mathbf{U}_{s,0}^{(1)} = \mathbf{A}_0^{(t1)}\mathbf{T}, \quad \mathbf{U}_{s,0}^{(2)} = \mathbf{A}_0^{(t2)}\mathbf{T}. \tag{17.67}$$

$\mathbf{A}_0^{(t2)}$ and $\mathbf{A}_0^{(t1)}$ differ due to the antenna position and thus are related by

$$\mathbf{A}_0^{(t2)} = \mathbf{A}_0^{(t1)}\mathbf{\Phi}_{[t]}, \tag{17.68}$$

where $\mathbf{\Phi}_{[t]}$ is a diagonal matrix with diagonal elements $[\mathbf{\Phi}_{[t]}]_{i,i} = \exp(j2\pi d_t \sin(\theta_i)/\lambda)$, $i = 1, ..., L_0$. Similarly, $\mathbf{U}_{s,0}^{(1)}$ and $\mathbf{U}_{s,0}^{(2)}$ are related by

$$\mathbf{U}_{s,0}^{(2)} = \mathbf{U}_{s,0}^{(1)}\mathbf{\Psi}_{[t]}. \tag{17.69}$$

From the above results, $\mathbf{\Psi}_{[t]}$ can be obtained from $\mathbf{U}_{s,0}^{(1)}$ and $\mathbf{U}_{s,0}^{(2)}$. Substituting (17.68) into (17.69), we obtain

$$\mathbf{U}_{s,0}^{(1)} = \mathbf{A}_0^{(t1)}\mathbf{T}, \quad \mathbf{U}_{s,0}^{(2)} = \mathbf{A}_0^{(t1)}\mathbf{\Phi}_{[t]}\mathbf{T}. \tag{17.70}$$

Therefore, it is concluded from (17.69) and (17.70) that $\mathbf{\Psi}_{[t]}$ and $\mathbf{\Phi}_{[t]}$ are related by $\mathbf{\Psi}_{[t]} = \mathbf{T}^{-1}\mathbf{\Phi}_{[t]}\mathbf{T}$, that is, $\mathbf{\Phi}_{[t]}$ can be obtained as the eigenvalues of $\mathbf{\Psi}_{[t]}$. As such, the DODs θ_i can be obtained for $i = 1, .., L_0$.

To estimate the DOAs after DODs are obtained, the ESPRIT-MUSIC method is based on the fact that noise subspace and the steering vector of the virtual array are orthogonal [21]. In the t-f framework, this leads to a t-f MUSIC based approach for each estimated θ_i, $i = 1, ..., L_0$, i.e., estimating the paired ϕ_i by finding the peaks of the following pseudo spatial spectrum

$$f(\phi) = \frac{1}{\mathbf{a}_r^H(\phi)[\mathbf{a}_t(\theta_i) \otimes \mathbf{I}_{N_r}]^H \mathbf{U}_{n,0} \mathbf{U}_{n,0}^H [\mathbf{a}_t(\theta_i) \otimes \mathbf{I}_{N_r}] \mathbf{a}_r(\phi)}. \tag{17.71}$$

When the receive array is uniform linear, for which the receive steering vector can be expressed as a polynomial function of $z = \exp(-j2\pi d_r \sin(\phi)/\lambda)$, i.e.,

$$\mathbf{a}_r(\phi) = [1, e^{-\frac{j2\pi d_r}{\lambda}\sin(\phi)}, ..., e^{-\frac{j2\pi(N_r-1)d_r}{\lambda}\sin(\phi)}]^T = [1, z, ..., z^{N_r-1}]^T, \tag{17.72}$$

the paired DOA ϕ_i can be solved using the simpler t-f root-MUSIC approach that finds the root inside and closest to the unit circle of the following polynomial

$$\mathbf{a}_r^H(\phi)[\mathbf{a}_t(\theta_i) \otimes \mathbf{I}_{N_r}]^H \mathbf{U}_{n,0} \mathbf{U}_{n,0}^H [\mathbf{a}_t(\theta_i) \otimes \mathbf{I}_{N_r}] \mathbf{a}_r(\phi) = 0. \tag{17.73}$$

For the directions of other $L - L_0$ targets, the same procedure can be carried out in different t-f regions where these signals are included.

By exploiting source selection/discrimination through t-f region selection, significant performance improvement can be achieved. This is particularly true in the challenging situations when multiple targets are closely spaced in angle but are separable in the time-frequency domain. Specifically, when a t-f region corresponding to a single target is identified, the DOD and DOA can be estimated with simple phase examinations, and no paring operation is needed.

Example

Consider a scenario in which two moving targets appear in a specific range bin of interest. The bistatic radar consists of a linear transmit array consisting of $N_t = 4$ antennas and a linear receive array of $N_r = 6$ antennas. The transmit and receive arrays are assumed to be distantly separated. Half wavelength interelement spacing is set for both transmit and receive arrays. The waveforms emitted from different transmit antennas are considered orthogonal, i.e., their crosscorrelations are ignored. The total number of samples is 256 for each waveform. The two targets have close DODs (10^o and 15^o) and DOAs (5^o and 20^o). The input SNR of all the return signals are assumed to be identical. The start frequencies of the two chirp signals is 0.15 and 0.18, and the respective ending frequencies are 0.35 and 0.38. The increasing Doppler signature of each target indicates the target movement towards the transmit and receive arrays in a way that the sum two-way slant range decreases over time.

In Figure 17.9, the root-mean-square error (RMSE) of the DOD and DOA estimation results of the first target are compared for three different scenarios, namely, joint ESPRIT-MUSIC without the use of time-frequency analysis, time-frequency ESPRIT-MUSIC with both signals selected for consideration, and time-frequency ESPRIT-MUSIC that only considers the signal corresponding to the first target. The results are averaged over 100 independent trials. It is evident that when both signals are selected, the t-f ESPRIT-MUSIC still benefits from the SNR enhancement over low SNR regions. It is also clear that the performance of both DOD and DOA estimates is significantly improved through target discrimination by considering only the first target. This improvement stems from overcoming the close angular separation of the targets at both the transmitter and receiver sides using t-f signature selections.

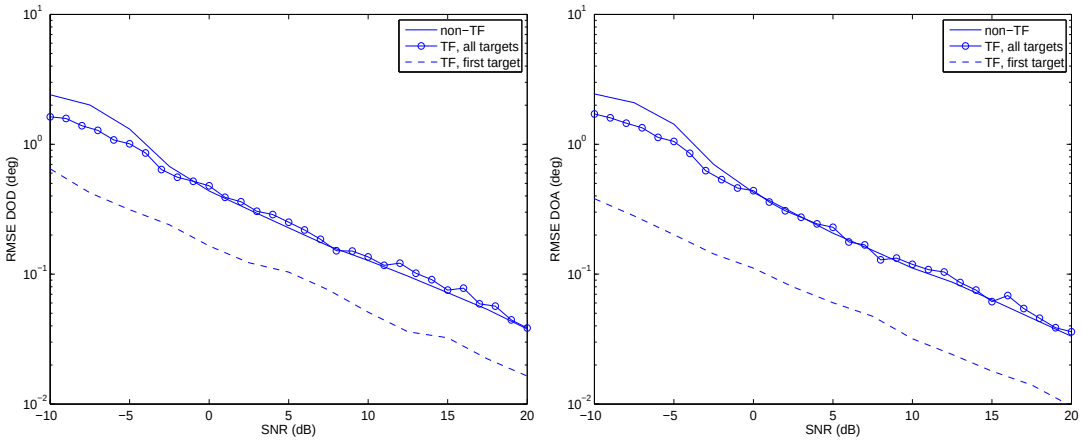

(a) DOD estimation (b) DOA estimation

Figure 17.9: Comparison of RMSE performance.

17.6 Conclusion

This Chapter discussed direction of arrival estimation of nonstationary signals that are characterized by instantaneous frequency laws. Conventional direction finding methods, including high resolution techniques, do not properly account for the instantaneous frequency characterization of the signals impinging on the antenna arrays. We discussed the spatial time-frequency distribution (STFD) framework which permits eigenstructure subspace methods to utilize the signal-to-noise ratio enhancement, brought about by incorporating the time-frequency regions of high power concentration. The latter are typically found at and around the signal time-frequency signature. High SNR data enable robustness of DOA estimates. It was also shown that distinction in the time-frequency signatures of closely spaced sources provides a discriminatory capability, within the STFD framework, which allows reducing the number of sources in the field of view to a single, or a subgroup of the sources. This permits processing more sources than sensors and reduces the variance of the source angular estimate. We extended the STFD framework to include multiple-input multiple-output (MIMO) configurations and estimated both the source direction-of-departure and direction-of-arrival. Although the focus of the chapter was on bilinear distributions of nonstationary signals, we also addressed linear time-frequency methods and their applications to DOA estimation of polynomial phase sources.

17.7 References

[1] L. B. Almeida, "The fractional Fourier transform and time-frequency representations," *IEEE Trans. signal Proc.*, vol. 42, no. ll, pp. 3084–3091, 1994.

[2] M. G. Amin, "Time-frequency spectrum analysis and estimation for nonstationary random processes, in B. Boashash (Ed), *Time-Frequency Signal Analysis: Methods and Applications*, Longman Cheshire, 1992.

[3] M. G. Amin, "Minimum variance time-frequency distribution kernels for signal in additive noise," *IEEE Trans. Signal Proc.*, vol. 44, no. 9, pp. 2352–2356, Sept. 1996.

[4] M. G. Amin, "Interference mitigation in spread spectrum communication systems using time-frequency distributions," *IEEE Trans. Signal Proc.*, vol. 45, no. 1, pp. 90–101, Jan. 1997.

[5] M. G. Amin, "Spatial time-frequency distributions for direction finding and blind source separation," *Proc. SPIE Wavelet Conf.*, Orlando, FL, April 1999.

[6] M. G. Amin, A. Belouchrani, and Y. Zhang, "The spatial ambiguity function and its applications," *IEEE Signal Proc. Lett.*, vol. 7, no. 6, pp. 138–140, June 2000.

[7] F. Auger, P. Flandrin, P. Gonçalvés, and O. Lemoine, *Time-Frequency Toolbox for Use with Matlab*. Available at http://tftb.nongnu.org/tutorial.pdf

[8] M. G. Amin and Y. Zhang, "Direction finding based on spatial time-frequency distribution matrices," *Digital Signal Proc.*, vol. 10, no. 4, pp. 325–339, Oct. 2000.

[9] M. G. Amin and Y. Zhang, "Spatial time-frequency distributions and their applications," in B. Boashash (ed.), *Time-Frequency Signal Analysis and Processing*, Oxford, UK: Elsevier, 2003.

[10] M. G. Amin and Y. Zhang, "Spatial time-frequency distributions and DOA estimation," in E. Tuncer and B. Friedlander (eds), *Classical and Modern Direction of Arrival Estimation*, Burlington, MA: Academic Press, 2009.

[11] M. G. Amin, Y. Zhang, G. J. Frazer, and A. R. Lindsey, "Spatial time-frequency distributions: Theory and applications," in L. Debnath (ed.), *Wavelets and Signal Processing*, Boston, MA: Birkhauser, 2003.

[12] A. Belouchrani and M. G. Amin, "Blind source separation based on time-frequency signal representations," *IEEE Trans. Signal Proc.*, vol. 46, no. 11, pp. 2888–2897, Nov. 1998.

[13] A. Belouchrani and M. G. Amin, "Time-frequency MUSIC," *IEEE Signal Proc. Lett.*, vol. 6, no. 5, pp. 109–110, May 1999.

[14] A. Belouchrani, M. G. Amin, N. Thirion-Moreau, and Y. D. Zhang, "Source separation and localization using time-frequency distributions," *IEEE Signal Proc. Mag.*, in press.

[15] S. Barbarossa, "Analysis of multicomponent LFM signals by a combined Wigner-Hough transform," *IEEE Trans. Signal Proc.*, vol. 43, no. 6, pp. 1511–1515, June 1995.

[16] S. Barbarossa, A. Scaglione, and G. B. Giannakis, "Product high-order ambiguity function for multicomponent polynomial-phase signal modeling," *IEEE Trans. Signal Proc.*, vol. 46, no. 3, pp. 691–708, March 1998.

[17] R. G. Baraniuk and D. L. Jones, "A signal-dependent time-frequency representation: optimal kernel design," *IEEE Trans. Signal Proc.*, vol. 41, pp. 1589–1602, April 1993.

[18] S. Barbarossa and O. Lemoine, "Analysis of nonlinear FM signals by pattern recognition of their time-frequency representation," *IEEE Signal Proc. Lett.*, vol. 3, no. 4, pp. 112–115, April 1996.

[19] B. Boashash, "Theory of quadratic TFDs," in B. Boashash (ed.), *Time-Frequency Signal Analysis and Processing*, Oxford, UK: Elsevier, 2003.

[20] B. Boashash and G. R. Putland, "Discrete time-frequency distributions," in B. Boashash (ed.), *Time-Frequency Signal Analysis and Processing*, Oxford, UK: Elsevier, 2003.

[21] M. L. Bencheikh and Y. Wang, "Joint DOD-DOA estimation using combined ESPRIT-MUSIC approach in MIMO radar," *Electronics Lett.*, vol. 46, no. 15, July 2010.

[22] L. Cohen, "Time-frequency distributions - a review," *Proc. IEEE*, vol. 77, no. 7, pp. 941–981, July 1989.

[23] L. Cohen, *Time-Frequency Analysis*, Englewood Cliffs, NJ: Prentice Hall, 1995.

[24] J. Chen, H. Gu, and W. Su, "A new method for joint DOD and DOA estimation in bistatic MIMO radar," *Signal Proc.*, vol. 90, pp. 714–719, 2010.

[25] H. I. Choi and W. J. Williams, "Improved time-frequency representation of multicomponent signals using exponential kernels," *IEEE Trans. Acoust., Speech, Sig. Proc.*, vol. ASSP-37, no. 6, pp. 862–871, June 1989.

[26] C. Duofang, C. Baixiao, and Q. Guodong, "Angle estimation using ESPRIT in MIMO radar," *Electronics Letters*, vol. 44, no. 12, June 2008.

[27] S. Djukanović, M. Daković, and L. Stanković, "Local polynomial Fourier transform receiver for nonstationary interference excision in DSSS communications," *IEEE Trans. Signal Proc.*, vol. 56, no. 4, pp. 1627–1636, 2008.

[28] S. Das and I. Pan, *Fractional Order Signal Processing: Introductory Concepts and Applications,* Springer, 2012.

[29] E. Fisher, A. Haimovich, R. Blum, D. Chizhik, L. Cimini, and R. Valenzuela, "MIMO radar: an idea whose time has come," *Proc. IEEE Radar Conf.*, pp. 71–78, April 2004.

[30] B. Friedlander and J. Weiss, "Direction finding for wide-band signals using an interpolated array," *IEEE Trans. Signal Proc.*, vol. 41, pp. 1618–1634, April 1993.

[31] A. Gershman and M. G. Amin, "Wideband direction-of-arrival estimation of multiple chirp signals using spatial time-frequency distributions," *IEEE Signal Proc. Lett.*, vol. 7, no. 6, pp. 152–155, June 2000.

[32] S. Hearon and M. G. Amin, "Minimum variance time-frequency distribution kernels, *IEEE Trans. Signal Proc.*, vol. 43, pp. 1258–1262, May 1995.

[33] A. Hassanien, A. B. Gershman, and M. G. Amin, "Time-frequency ESPRIT for direction-of-arrival estimation of chirp signals," in *Proc. IEEE Sensor Array and Multichannel Signal Processing Workshop*, Rosslyn, VA, pp. 337–341, Aug. 2002.

[34] A. Hassanien, S. A. Vorobyov, and A. B. Gershman, "Moving target parameters estimation in noncoherent MIMO radar systems," *IEEE Trans. Signal Proc.*, vol. 60, no. 5, pp. 2354–2361, May 2012.

[35] C. Ioana and A. Quinquis, "Time-frequency analysis using warped-based high-order phase modeling," *EURASIP J. Applied Signal Proc.*, vol. 2005, no. 17, pp. 2856–2873, Sept. 2005.

[36] C. Ioana, Y. D. Zhang, M. G. Amin, F. Ahmad, and B. Himed, "Time-frequency analysis of multipath Doppler signatures of maneuvering targets," in *Proc. IEEE Int. Conf. Acoustics, Speech, Signal Proc.*, Kyoto, Japan, March 2012.

[37] C. Ioana, Y. D. Zhang, M. G. Amin, F. Ahmad, G. Frazer, and B. Himed, "Time-frequency characterization of micro-multipath signals in over-the-horizon radar," in *Proc. IEEE Int. Radar Conf.*, Atlanta, GA, pp. 671–675, May 2012.

[38] M. Jin, G. Liao, and J. Li, "Joint DOD and DOA estimation for bistatic MIMO radar," *Signal Proc.*, vol. 89, pp. 244–251, 2009.

[39] J. Jeong and W. J. Williams, "Kernel design for reduced interference distributions," *IEEE Trans. Signal Proc.*, vol. 42, pp. 402–412, 1992.

[40] N. Linh-Trung, A. Belouchrani, K. Abed-Meraim, and B. Boashash, "Separating more sources than sensors using time-frequency distributions," *EURASIP J. Applied Signal Proc.*, vol. 2005, no. 17, pp. 2828–2847, 2005.

[41] W. Li, "Wigner distribution method equivalent to dechirp method for detecting a chirp signal," *IEEE Trans. Acoust. Speech, Signal Proc.*, vol. ASSP-35, pp. 1210–1211, Aug. 1987.

[42] J. Li and P. Stoica, "MIMO radar with colocated antennas," *IEEE Signal Processing Mag.*, vol. 25, no. 5, pp. 106–114, Sept. 2007.

[43] J. Li and P. Stoica (Eds.), *MIMO Radar Signal Processing,* New York, NY: Wiley-IEEE Press, 2009.

[44] W. Mu and M. G. Amin, "SNR analysis of time-frequency distributions," in *Proc. IEEE Int. Conf. Acoust., Speech, Sig. Proc.*, Istanbul, Turkey, pp. II645–II648, June 2000.

[45] W. Mu, M. G. Amin, and Y. Zhang, "Bilinear signal synthesis in array processing," *IEEE Trans. Signal Proc.*, vol. 51, no. 1, pp. 90–100, Jan. 2003.

[46] N. Ma and J. T. Goh, "Ambiguity-function-based techniques to estimate DOA of broadband chirp signals," *IEEE Trans. Signal Proc.*, vol. 54, no. 5, pp. 1826–1839, May 2006.

[47] V. Namias, "The fractional order Fourier transform and its application to quantum mechanics," *J. Inst. Math. Appl.*, vol. 25, pp. 241–265, 1980.

[48] B. A. Obeidat, Y. Zhang, and M. G. Amin, "DOA and polarization estimation for wideband sources," in *Proc. Asilomar Conf. Signals, Sys., Comput.*, Pacific Grove, CA, Nov. 2004.

[49] A. Papandreou-Suppappola, *Applications in Time-Frequency Signal Processing*, Boca Raton, FL: CRC Press, 2003.

[50] B. Porat, *Digital Processing of Random Signals: Theory and Methods*, Englewood Cliffs, NJ: Prentice Hall, 1993.

[51] S. Peleg and B. Porat, "Estimation and classification of polynomial-phase signals," *IEEE Trans. Inform. Theory*, vol. 37, March 1991.

[52] D. S. Pham and A. M. Zoubir, "Analysis of multicomponent polynomial phase signals," *IEEE Trans. Signal Proc.*, vol. 55, no. 1, pp. 56–65, Jan. 2007.

[53] S. Qian and D. Chen, *Joint Time-Frequency Analysis - Methods and Applications*, Englewood Cliffs, NJ: Prentice Hall, 1996.

[54] H. Qu, R. Wang, W. Qu, and P. Zhao, "Research on DOA estimation of multi-component LFM signals based on the FRFT," *Wireless Sensor Network*, vol. 2009, no. 3, pp. 171–181, 2009.

[55] S. Rickard and F. Dietrich, "DOA estimation of many W-disjoint orthogonal sources from two mixtures using DUET," in *Proc. IEEE Workshop on Statistical Signal and Array Processing*, Pocono, PA, pp. 311–314, Aug. 2000.

[56] R. Roy and T. Kailath, "ESPRIT-estimation of signal parameters via rotational invariance techniques," *IEEE Trans. Acoust., Speech, Sig. Proc.*, vol. ASSP-37, no. 7, pp. 984–995, July 1989.

[57] R. O. Schmidt, "Multiple emitter location and signal parameter estimation," *IEEE Trans. Antennas Propagat.*, vol. AP-34, no. 3, pp. 276–280, March 1986.

[58] P. Stoica and A. Nehorai, "MUSIC, maximum likelihood and Cramer-Rao bound," *IEEE Trans. Acoust., Speech, Sig. Proc.*, vol. ASSP-37, no. 5, pp. 720–741, May 1989.

[59] K. Sekihara, S. Nagarajan, D. Poeppel, and Y. Miyashita, "Time-frequency MEG-MUSIC algorithm," *IEEE Trans. Medical Imaging*, vol. 18, no. 1, pp. 92–97, Jan. 1999.

[60] L. Stankovic, "A time-frequency distribution concentrated along the instantaneous frequency, *IEEE Signal Proc. Lett.*, vol. 3, no. 3, pp. 89-91, March 1996.

[61] L. Stankovic, "Analysis of noise in time-frequency distributions," *IEEE Signal Proc. Lett.*, vol. 9, no. 9, pp. 286-289, Sept. 2002.

[62] J. C. Wood and D. T. Barry, "Radon transformation of time-frequency distributions for analysis of multicomponent signals," *IEEE Trans. Signal proc.*, vol. 42, no. 11, pp. 3166–3177, Nov. 1994.

[63] N. J. Willis and H. D. Griffiths (eds), *Advances in Bistatic Radar*, SciTech Publishing, 2007.

[64] H. Wang and M. Kaveh, "Coherent signal-subspace processing for the detection and estimation of angles of arrival of multiple wideband sources," *IEEE Trans. Acoust., Speech, Sig. Proc.*, vol. ASSP-33, pp. 823–831, Aug. 1985.

[65] G. Wang and X.-G. Xia, "Iterative algorithm for direction of arrival estimation with wideband chirp signals," *IEE Proc. Radar, Sonar Navig.*, vol. 147, no. 5, pp. 233–238, Oct. 2000.

[66] Q. Wang and C. Wu, "A high reliability DOA estimation method – TF-ESPRIT method," in *Proc. Int. Conf. Signal Proc.*, Beijing, China, pp. 374–377, Aug. 2002.

[67] X-G. Xia and V. Chen, "A quantitative SNR analysis for the pseudo Wigner-Ville distribution," *IEEE Trans. Signal Proc.*, vol. 47, no. 10, pp. 2891–2894, Oct. 1999.

[68] Y. Zhang and M. G. Amin, "Blind separation of nonstationary sources based on spatial time-frequency distributions," *EURASIP J. Applied Signal Proc.*, vol. 2006, article ID 64785, 13 pages, 2006.

[69] Y. D. Zhang, M. G. Amin, and B. Himed, "Joint DOD/DOA Estimation in MIMO Radar Exploiting Time-Frequency Signal Representations," *EURASIP J. Advanced Sig. Proc.*, vol. 2012, no. 1, 2012:102.

[70] Y. D. Zhang, M. G. Amin, and B. Himed, "Altitude estimation of maneuvering targets in MIMO over-the-horizon radar," *IEEE Sensor Array and Multichannel Signal Processing Workshop*, Stevens, NJ, pp. 261–264, June 2012.

[71] Y. D. Zhang, M. G. Amin, and B. Himed, "Direction-of-arrival estimation of nonstationary signals exploiting signal characteristics," *Int. Conf. Inform. Science Signal Proc. Their Applications*, Montreal, Canada, July 2012.

[72] Y. Zhao, L. E. Atlas, and R. J. Marks, "The use of cone-shaped kernels for generalized time-frequency representations of non-stationary signals," *IEEE Trans. Acoust., Speech, and Sig. Proc.*, vol. ASSP-38, pp. 1084–1091, July 1990.

[73] Y. Zhang, G. J. Frazer, and M. G. Amin, "Concurrent operation of two over-thehorizon radars," *IEEE J. Sel. Topics Signal Process.*, vol. 1, no. 1, pp. 114-123, June 2007.

[74] Y. Zhang, W. Mu, and M. G. Amin, "Time-frequency maximum likelihood methods for direction finding," *J. Franklin Inst.*, vol. 337, no. 4, pp. 483–497, July 2000.

[75] Y. Zhang, W. Mu, and M. G. Amin, "Subspace analysis of spatial time-frequency distribution matrices," *IEEE Trans. Signal Proc.*, vol. 49, no. 4, pp. 747–759, April 2001.

[76] I. Ziskind and M. Wax, "Maximum likelihood localization of multiple sources by alternating projection," *IEEE Trans. Acoust. Speech Sig. Process.*, vol. ASSP-36, no. 10, pp. 1553–1560, Oct. 1988.